IEEE Access
Multidisciplinary | Rapid Review | Open Access Journal

Received July 13, 2021, accepted August 24, 2021, date of publication September 23, 2021, date of current version October 5, 2021.

Digital Object Identifier 10.1109/ACCESS.2021.3115425

ProLab: A Perceptually Uniform Projective Color Coordinate System

IVAN A. KONOVALENKO[1,2], ANNA A. SMAGINA[1], DMITRY P. NIKOLAEV[1,2], (Member, IEEE), AND PETR P. NIKOLAEV[1,3]

[1]Institute for Information Transmission Problems (IITP), Russian Academy of Sciences, 127051 Moscow, Russia
[2]Smart Engines Service LLC, 117312 Moscow, Russia
[3]Moscow Institute of Physics and Technology (MIPT), 141700 Dolgoprudny, Moscow, Russia

Corresponding author: Dmitry P. Nikolaev (dimonstr@iitp.ru)

This work was supported in part by RFBR under the Scientific Project 17-29-03370 and the Scientific Project 19-29-09075.

ABSTRACT The construction of perceptually uniform color space is an important task of color theory. Many image processing applications requires the color difference to replicate human perception. The perceptual difference is poorly approximated by Euclidean distance within linear color coordinate systems, in particular, within CIE XYZ. Almost all uniform color spaces are constructed as some nonlinear transformation from CIE XYZ. Such transformations do not preserve the straightness of the color tone curves and other collinearity properties which are important for high dynamic range and wide color gamut imagery and required for linear color analysis, including separation of homogeneous backgrounds. In this work, we propose proLab, a new color coordinate system derived as a 3D projective transformation of CIE XYZ that preserves the linearity of manifolds by definition. We show that proLab is far superior to the widely used CIELAB coordinate system (though inferior to the modern CAM16-UCS) in terms of perceptual uniformity, evaluated by the STRESS metric in reference to the CIEDE2000 color difference formula. We also demonstrate that shot noise in proLab is more homoscedastic than in CAM16-UCS or other standard color spaces. This makes proLab a convenient coordinate system for linear color analysis.

INDEX TERMS Color, mathematical model, linearity, image representation, image color analysis, noise measurement.

I. INTRODUCTION

The purpose of this work is to develop a new color coordinate system for the analysis of color images of the visible light spectrum. Most existing algorithms for color analysis operate with distances in a color space, and some of them rely on the linear properties of color distributions. On the other hand, the color space metric, as a rule, is not derived strictly from physical models but rather from the properties of human color perception using psychophysiological experimental data. The color coordinate system proposed in this work is based on the color perception model as well as on physical models of image formation; thus, for an accurate problem statement, we have to provide a detailed introduction. Sections I-A and I-B are dedicated to color models in psychophysics; Sections I-C and I-D, to the aspects of color image formation and processing. Then, in Section I-E, we formulate the problem to be solved and propose the general idea of the solution. Section I-F addresses the most relevant works in the field. In Section I-G, the desired properties of the proposed coordinate system are listed.

The associate editor coordinating the review of this manuscript and approving it for publication was Ananya Sen Gupta.

A. COLOR SPACES AND COLOR COORDINATE SYSTEMS

The human perception of color is defined by the spatial distribution of retinal irradiance and the internal state of the visual system. Under photopic conditions, there are three types of active cones, the reactions of which can be considered continuously dependent on the irradiance. Under the assumption that photoreceptors are negligibly small and uniformly distributed, the response to the irradiance at each point on the retina can be represented as three scalar reactions. All other elements of the visual system employ not arbitrary parameters of the irradiance but rather these three scalar reactions exclusively. In this model, given a fixed internal state, the color perception caused by a uniformly illuminated part of the retina depends on a 3D manifold, regardless of the visual system's complexity and its internal state. We call this manifold a color space, and its elements we call colors.

This work is licensed under a Creative Commons Attribution 4.0 License. For more information, see https://creativecommons.org/licenses/by/4.0/

To perform color mapping, various color coordinate systems are used. In any of them, the coordinates of the color vector $\mathbf{c}$ are related to the spectral irradiance $F(\lambda)$ through some vector functional Ψ, which can be additionally parameterized with context information and the internal state $\boldsymbol{\theta}$ of the visual system:

$$\mathbf{c} = \Psi_{\boldsymbol{\theta}}[F(\lambda)], \tag{1}$$

where λ is the light wavelength. The color coordinate space is called linear if Ψ is linear for fixed $\boldsymbol{\theta}$.

In 1853, Grassmann showed [1] that under colorimetric conditions, a linear 3D color coordinate system of the human vision system can be constructed, while the internal state of the latter can be neglected due to these conditions. This discovery reduced the problem of determining the color space for the human eye to a linear-color-coordinate-based construction in the spectral irradiance space $F(\lambda)$. In this system, the relationship between the retinal spectral irradiance and the color coordinates is constructed analytically:

$$\mathbf{c_x} \stackrel{\text{def}}{=} \int_0^\infty F(\lambda)\mathbf{X}(\lambda)d\lambda, \tag{2}$$

where $\mathbf{X}(\lambda)$ denotes the color matching functions of a standard observer and $\mathbf{c_x}$ denotes the color coordinates in CIE XYZ.

Thus far, various color coordinate systems have been proposed for the standard observer. These systems vary in terms of their suitability for specific applications [2]. Some of them imply colorimetric conditions. Others are related to the various color perception models, which parameterize $\boldsymbol{\theta}$ in one way or another. Assuming that the visual context and the internal state do not affect the spectral sensitivity, the coordinate vectors in any of these coordinate systems can be expressed via CIE XYZ coordinates independently of $F(\lambda)$:

$$\mathbf{c_\Phi} = \Psi_{\Phi,\boldsymbol{\theta}}[F(\lambda)] = \Phi_{\boldsymbol{\theta}}(\mathbf{c_x}), \tag{3}$$

where $\Phi_{\boldsymbol{\theta}}$ is the transformation from CIE XYZ to the given coordinate system under known internal state $\boldsymbol{\theta}$.

Usually, color perception models consider at least the adaptation of the visual system to the dominant illuminance [3]. In von Kries' model [4], this is expressed within the transformation (3) as a componentwise division of the input coordinate vector $\mathbf{c_x}$ by the light source color coordinate vector $\mathbf{c_x^*}(\boldsymbol{\theta})$:

$$\Phi_{\boldsymbol{\theta}}(\mathbf{c_x}) = \Phi_{\mathbf{0}}\left(\operatorname{diag}\left(\mathbf{c_x^*}\,(\boldsymbol{\theta})\right)^{-1}\mathbf{c_x}\right), \tag{4}$$

where $\Phi_{\mathbf{0}}$ is a transformation that is independent of the illumination.

In systems with the same adaptation model, the coordinate transformation could be performed while bypassing CIE XYZ, and obviously, this transformation does not require information on the illumination:

$$\begin{cases} \mathbf{c_a} = \mathrm{A}_{\boldsymbol{\theta}}(\mathbf{c_x}) \stackrel{\text{def}}{=} \mathrm{A}_{\mathbf{0}}\left(\operatorname{diag}\left(\mathbf{c_x^*}\,(\boldsymbol{\theta})\right)^{-1}\mathbf{c_x}\right) \\ \mathbf{c_b} = \mathrm{B}_{\boldsymbol{\theta}}(\mathbf{c_x}) \stackrel{\text{def}}{=} \mathrm{B}_{\mathbf{0}}\left(\operatorname{diag}\left(\mathbf{c_x^*}\,(\boldsymbol{\theta})\right)^{-1}\mathbf{c_x}\right) \end{cases} \Longrightarrow \mathbf{c_b} = \mathrm{B}_{\mathbf{0}}\left(\mathrm{A}_{\mathbf{0}}{}^{-1}(\mathbf{c_a})\right), \tag{5}$$

where $\mathbf{c_a}$ and $\mathbf{c_b}$ are the color coordinate vectors in the two coordinate systems, defined by the transformations $\mathrm{A}_{\boldsymbol{\theta}}$ and $\mathrm{B}_{\boldsymbol{\theta}}$, respectively.

B. EVALUATION METRIC AND PERCEPTUAL UNIFORMITY

Psychophysical experiments not only reveal the spectral basis of the color space perceived by people but also help to determine its metric parameters. This can be done, for instance, by measuring changes in the thresholds in spectral stimuli for a human eye at different points of the color space. The color coordinate space is called perceptually uniform (hereinafter – uniform) if the Euclidean distances between the colors in it correspond to the differences perceived by the human eye. Liminal difference vector lengths are uniform across all of the points and in any direction in this space. The CIE XYZ linear coordinate system provides a color space with a natural Euclidean representation, but it is significantly nonuniform in this regard.

There have been many attempts to create a uniform color coordinate space. In 1948, Richard Hunter proposed the first uniform space, Hunter Lab [5]. Later, David MacAdam proposed a space based on a study by Dean Judd [6]. This space was standardized by CIE in 1960 as a uniform chromaticity space (CIE 1960 UCS). As its name implies, this coordinate system does not include any brightness component. Soon after that, Gunter Wyszecki proposed a space [7] based on the latter one, which was adopted as the CIE 1964 (U*, V*, W*) color space (or CIEUVW). It allowed for the calculation of the color differences even with mismatched brightness. In 1976, the CIELAB space was developed based on Hunter Lab [8]. It is still the most used uniform color coordinate system when it comes to complex stimuli (images) analysis.

However, the CIELAB space is only approximately uniform, so from the moment of its inception, there have been continuous attempts to create more uniform coordinate systems (e.g., [9]). At the same time, non-Euclidean color difference formulas were being developed to provide more precise correlation with experiments regarding human perception. The successful outcome of these efforts was the CIEDE2000 formula [10], [11], which is still considered the most accurate one available [12]. Nevertheless, for some applications, it is preferable to operate in color coordinate spaces with a uniform Euclidean distance (e.g., for the development of effective search structures). Therefore, uniform spaces are still being actively researched and developed. Currently, the CAM16-UCS space [13], developed in 2016, is considered to be the accuracy standard among these.

C. COLOR SPACES OF VISIBLE-SPECTRUM CAMERAS

With certain reservations, all of the aforesaid can also be attributed to technical visual systems. Of course, we are not considering the perception of technical systems. In technical vision systems, the term 'color' usually means a 3D vector that is passed on for further processing. In addition, the internal state $\boldsymbol{\theta}$ of these systems, as a rule, could be neglected or considered to be known. However, the most important thing

is that the spectral basis of the camera space is significantly different from those of the standard observer. Moreover, the color spaces of cameras made by different manufacturers are usually mismatched.

To use the color coordinates of one color space within another one, a mapping between these color spaces must be built. This concept is invalid in the general case: an element of any color space corresponds to an infinite set of metameric spectral irradiance; this set can be mapped into a set of significant volume of the different color space.

The quality of color reproduction under different conditions depends on the choice of a particular mapping. Various mathematical models have been proposed for its construction. The most commonly used is a linear one [14]. Nonlinear color mappings – polynomial [15] and root-polynomial [16] – are also well known. Both of these show better accuracy in experiments. The latter model is also invariant to changes in brightness, similar to the linear model. In [17], an interesting approach is discussed: the linear mapping parameters are considered to be dependent on the dominant illumination estimation. The latter is obtained via analysis of the input image using some algorithm (the dependency of $\boldsymbol{\theta}$ is established). Moreover, in [18], possible refinements of the experimental pipeline are proposed, and in [19], the choice of loss function to be minimized for model fitting is discussed.

When dealing with mass-market visible-light cameras, the calibration transformation into the standard observer color space is considered to be known, which allows for the assignment of the human color space coordinates to the captured colors. As a rule, the method for the evaluation of the transformation parameters and, sometimes, the model of such a transformation itself are hidden from the user.

D. IMPORTANCE OF LINEAR MANIFOLDS IN COLOR IMAGE ANALYSIS

In technical systems, the algorithms for color image analysis and processing are based on both human color perceptual models and physical models of image formation. The most famous among the latter is probably the dichromatic reflection model proposed by Shafer [20]. This model assumes that the color distribution of the uniformly colored glossy dielectric surface, illuminated by a single source, forms a plane in the linear color coordinate space. The assertion of the linear degeneration of the color distribution was already formulated early on, at least by 1975 [21], but Shafer's model additionally specifies the shape of the color distribution on the plane. This model was further developed and generalized, resulting in the expansion of the list of conditions under which the color distributions of uniformly colored objects form linear manifolds of various dimensions [22], [23]. We call all the models of this family linear models of color image formation.

Linear models are used, for instance, in color-based image segmentation [23]–[26], as well as in computational color constancy. The main problem of the latter is to estimate the color of the light source of a scene. One of the ways to solve this is to find the intersection of two dichromatic planes in the linear color coordinate space. According to the linear model, the chromaticity of the direction vector of the planes' intersection is the same as the chromaticity of the dominant light source [27]. This technique is used in various color constancy algorithms [28], [29].

Note that in earlier works on this topic, only color distributions forming 2D linear subspaces were considered. However, the algorithms developed later consider a more realistic model that includes diffused light, where the considered manifolds do not pass through the origin of the coordinates [30]. The generalized versions of this approach are used in the analysis of scenes with multiple light sources [23], [31] as well as in multispectral image analysis [32].

The assumption that the interaction of light with matter is linear leads to a more obvious and fundamental property – changes in integral illuminance brightness do not affect the chromaticity of image pixels regardless of the number of reflections in the scene, the coloring of the objects, and the chromaticity of the light source. This is what recovery [33]–[35] and reproduction angular errors [36], widely used in computational color constancy, are based on. The first metric considers the angle between the true color vector of the illuminance and its estimation. The second considers the angle between two color vectors, one of which is the color vector of a white surface under the given illumination, normalized channelwise by the estimated light source chromaticity, while the other corresponds to a white surface under an equal-energy illuminant (''true white point'').

These color constancy algorithms, based on linear manifold incidence along with angular accuracy errors, are applied to linear color coordinate spaces, since in nonlinear spaces, the relevant geometric properties of the color distribution are not preserved.

E. THE REASON BEHIND THE DEVELOPMENT OF NEW COLOR COORDINATES

The structural analysis of linear color distributions mainly includes two problems. The first one is to estimate the linear cluster parameters in a color space using regression methods, and the key factor here is the tolerance for color deviations caused by image noise. The second problem is the analysis of the mutual positioning of the detected manifolds in a color space. The algorithms for solving these problems employ the color differences directly. Thus, for applications where the behavior of these algorithms is expected to be in correspondence with human perception, the color difference metrics should preferably be in correspondence with the human ones.

When applying basic statistical methods to the color distribution of an image, the color noise is considered to be homoscedastic, i.e., the color deviations are additive, well approximated by a random variable with zero mean, distributed independently from the observed coordinates, and invariant to rotation. However, even affine transformations of color coordinates can affect the additive noise anisotropy. Nonlinear transformations can also make the parameters of

the color distribution dependent on the observed color coordinates. Thus, the correctness of the results obtained via basic statistical methods significantly depends on the coordinate system in which the color distributions are analyzed.

The problem is further complicated by the fact that image noise is not homoscedastic in the space of linear sensor responses [37]. This means that basic regression methods provide nonoptimal estimation of the color manifolds' positioning even in linear color spaces. As a result, both nonlinear and linear color spaces are poorly applicable for structural analysis: the physical models in perceptually uniform spaces are overcomplicated, and the noise is heteroscedastic [38], while in linear spaces, the errors do not correlate with human perceptual differences, and noise homoscedasticity is not guaranteed for linear spaces. The same goes for the problem of angular errors: in linear color spaces, deviations by the same angle in different directions are not guaranteed to be equally perceived by the human eye, while in perceptually uniform spaces, equal chromaticities form a curve; thus, the concept of angle is not very applicable here.

Thus, our goal is to construct a perceptually uniform space of color coordinates that preserves the linearity of subspaces and manifolds. Moreover, it is preferable that the sensor noise in this space be as homoscedastic as possible.

F. HOMOGRAPHY OF 3D COLOR COORDINATES

If the preservation of manifold linearity required linearity of the transformation, our goal would hardly be achievable. First, linear transformations cannot make noise more homoscedastic since the Jacobian matrix of a linear transformation is constant across the space. (However, it is possible to correct the noise anisotropy.) Moreover, linear transformations cannot significantly improve perceptual uniformity of the space: colors that are equally spaced in CIE XYZ coordinates are not perceptually uniform on the achromatic axis, and affine transformations preserve the ratio of segment lengths located along any line.

However, the class of transformations that preserve the linearity of the manifolds is much wider: it includes any projective transformations. Unlike affine transformations, projective ones allow for changes in the elements across the space in different ways. Figure 1 illustrates a projective transformation compressing the space in the vicinity of one point and stretching the space in the vicinity of another while keeping all of the lines straight. It suggests that a solution with acceptable uniformity is possible, i.e., a color coordinate system with the desired properties can be developed.

Projective transformations of color coordinates are already widely used in various applications [39]. However, projective transformations are usually applied only to the chromaticity plane. Apparently, MacAdam [40] was the first researcher who proposed projective transformations for the construction of a uniform color space, but in his pioneering work, as well as in later papers, only 2D transformations are considered.

In 2003, the first work introducing the transformation of the entire color space was published [41]. It employed a 3D projective transformation for color gamut matching for various projector devices. Later, the same approach was applied to photorealistic color transfer between images [42]. Both methods employ mutual calibration of two images rather than transformation into some reference space with a different metric. The latter method was used in [43]. This research demonstrated that a fixed 3D projective color coordinate transformation improves the results of color-based image segmentation [43]. In 2020, Kim *et al.* [44] employed a 3D projective transformation for the color calibration of micro-LED displays.

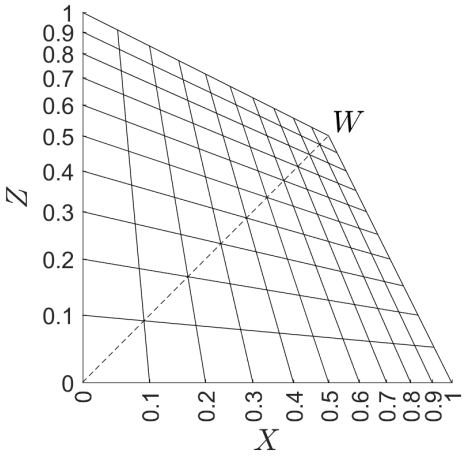

FIGURE 1. XZ plane of the CIE XYZ color coordinate system in the projective color coordinate space. Point W denotes the projection of the white point.

G. PROPOSED COLOR COORDINATE SYSTEM

In this work, we propose proLab, a uniform color coordinate system for the standard observer that is based on a 3D projective transformation of CIE XYZ coordinates. We demonstrate the following advantages of the new coordinate system:

- ProLab is far superior to the commonly used uniform system CIELAB in terms of perceptual uniformity (although it is inferior to CAM16-UCS).
- The image shot noise is more homoscedastic in proLab than in other uniform spaces.
- Among the uniform systems, proLab is the only one that preserves the linearity of color manifolds; this property allows for the employment of the angular accuracy of a color reproduction and for linear color analysis in accordance with a human color difference metric.
- The transformation from CIE XYZ to proLab has an elegant analytical expression, and it is computationally efficient compared with CAM16-UCS and the even more primitive CIELAB.

We presented the idea of constructing the proLab coordinate system for the first time at the 25th Symposium of the International Society for Color Vision in 2019 [45], but the construction methodology and a numerical study of the properties of proLab are discussed in detail for the first time in the current work. Moreover, the model parameters have

been estimated more accurately compared to those presented at the Symposium.

H. OUTLINE OF THE MAIN RESULTS: PAPER STRUCTURE

The main part of the article is organized as follows. Four sections are focused on the construction of the proLab coordinate system. In Section II, we introduce the necessary notation, construct the basic model of the transformation from CIE XYZ to proLab, and discuss how to determine the transformation parameters that do not affect the metric. In Section III, a priori restrictions on the proLab metric parameters are given. In Section IV, we introduce a function quantifying the perceptual uniformity of color coordinates. In Section V, we provide the optimal proLab parameters along with the step-by-step methodology to obtain them.

Then, we study the properties of the resulting color coordinate system. In Section VI, we propose a function to quantify the deviation of the color coordinate noise parameters from homoscedasticity. In Section VII, the noise model for the color sensor is constructed, and noise parameters estimated on a raw image from an open dataset are provided. In Section VIII, we provide a numerical comparison of the properties of proLab with those of the existing coordinate systems in terms of uniformity and noise homoscedasticity. In Section IX, we discuss several specific possible applications of the constructed coordinate system. In the Discussion, we review some qualitative properties of the proposed coordinate space and suggest possible optimizations of the parameters of proLab. In the Conclusions, the main results of this work are summarized.

II. BASICS OF THE PROLAB COLOR MODEL

Let us now construct a color coordinate space of the standard observer such that color manifolds that are linear in CIE XYZ will remain linear in the constructed space. In addition, we require the Euclidean distance in this space to approximate the color differences determined in a certain way.

Let us denote the CIE XYZ color coordinate space as C_x, the CIELAB coordinate space as C_l, and the constructed space as C_p. By L, we denote the transformation from C_x to C_l, and by P, from C_x to C_p. As follows from the requirement of linearity preservation of the manifolds, P is a 3D projective transformation. Let us parameterize any projective transformation in standard matrix notation, denoted by italics (e.g., matrix $P \stackrel{\text{def}}{=} (p_{ij}) \in \mathbb{R}^{4\times4}$ corresponds to the transformation P).

Let $\mathrm{T_h}$ and $\mathrm{T_c}$ be functions for the transformation between Cartesian and homogeneous coordinates:

$$\begin{aligned} \mathrm{T_h}(\mathbf{c}) &\stackrel{\text{def}}{=} \begin{bmatrix} \mathbf{c} \\ 1 \end{bmatrix}, \quad \mathbf{c} \in \mathbb{R}^3, \\ \mathrm{T_c}(\mathbf{h}) &\stackrel{\text{def}}{=} \begin{bmatrix} I_3 & \mathbf{0} \end{bmatrix} \frac{\mathbf{h}}{h_4}, \quad \mathbf{h} \in \mathbb{R}^4, \quad h_4 \neq 0, \end{aligned} \tag{6}$$

where I_3 is the 3×3 identity matrix. Then,

$$\mathrm{P}(\mathbf{c_x}) \stackrel{\text{def}}{=} \mathrm{T_c}\big(P\mathrm{T_h}(\mathbf{c_x})\big), \quad \mathbf{c_x} \in C_x, \quad \mathrm{P}(\mathbf{c_x}) \in C_p. \tag{7}$$

Any requirements on metrics over C_p define P only up to a similarity in C_p. Indeed, applying a rigid transformation to C_p does not change distances, while isotropic scaling is equivalent to a change in the distance-measuring units. To make the solution unique, we need to introduce some additional restrictions on P.

Let us build the coordinate system that could replace CIELAB in the simplest possible way. First, we require distances in C_p to model the dominant light source adaptation in the same way as in CIELAB. For this purpose, let us consider the simplified von Kries model [4], performing the componentwise division of the input vector coordinates $\mathbf{c_x}$ by the light source color coordinates $\mathbf{c}_\mathbf{x}^* \in C_x$. Let us denote the adaptation transformation as N. This transformation is projective, and its corresponding transformation matrix can be defined as:

$$N \stackrel{\text{def}}{=} \operatorname{diag}\left(\mathrm{T_h}\left(\mathbf{c}_\mathbf{x}^*\right)\right)^{-1}. \tag{8}$$

Now, P can be decomposed into the adaptation transformation N and the transformation Q independent of the dominant light source:

$$\mathrm{P} = \mathrm{Q} \circ \mathrm{N}, \quad P = QN, \quad Q \stackrel{\text{def}}{=} (q_{ij}) \in \mathbb{R}^{4\times4}, \tag{9}$$

where $\circ$ is the function composition operator. In addition, we require the black point $\mathbf{0}$ to be preserved by P:

$$\mathrm{P}(\mathbf{0}) = \mathbf{0}. \tag{10}$$

Then, Q can be written as follows:

$$Q(\boldsymbol{\varphi}, \rho, \boldsymbol{\mu}) = R_1(\varphi_1)R_2(\varphi_2)R_3(\varphi_3)Z(\rho)M(\boldsymbol{\mu}), \tag{11}$$

where $R_i(\varphi)$ is a matrix for rotation by an angle φ about an axis i, $Z(\rho)$ is the isotropic scaling matrix with a scaling factor $\rho > 0$, and $M(\boldsymbol{\mu})$ is a special matrix that defines the metric properties of C_p:

$$M(\boldsymbol{\mu}) \stackrel{\text{def}}{=} \begin{bmatrix} \mu_1 & \mu_2 & \mu_3 & 0 \\ 0 & \mu_4 & \mu_5 & 0 \\ 0 & 0 & 1 & 0 \\ \mu_6 & \mu_7 & \mu_8 & 1 \end{bmatrix}, \quad |M| > 0, \tag{12}$$

where $\boldsymbol{\mu} \in \mathbb{R}^8$ is a vector of the metric parameters.

Decomposition (11) allows us to determine the metric parameters $\boldsymbol{\mu}$ separately from the similarity parameters $\boldsymbol{\varphi}$ and ρ. Here, we do not consider mirroring of the coordinate system, as the simultaneous fulfillment of conditions $|M| > 0$ and $\rho > 0$ itself keeps the color hues' traversal order around the achromatic axis the same as in CIE XYZ and CIELAB. Note also that the matrices $R_i(\varphi)$ and $Z(\rho)$ are defined up to multiplication by a nonzero scalar. To define these matrices, we require the bottom-right element to be equal to one. Hence,

$$p_{44} = q_{44} = 1. \tag{13}$$

Consider the metric parameters $\boldsymbol{\mu}$ to be known. Now, let us fix the rest of the parameters. First, let us set the direction and overall scale of the lightness axis as in CIELAB:

$$\mathrm{P}\left(\mathbf{c}_\mathbf{x}^*\right) = \begin{bmatrix} 100 & 0 & 0 \end{bmatrix}^T. \tag{14}$$

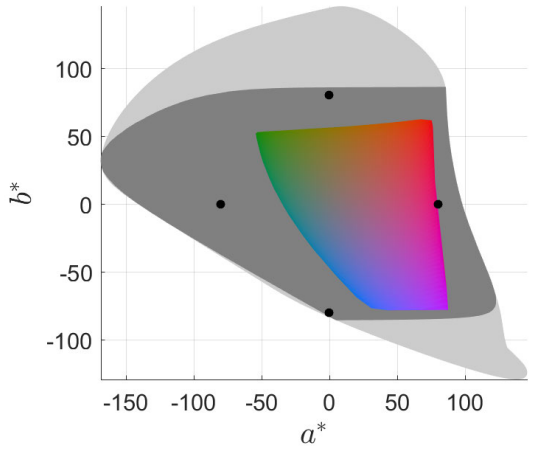

FIGURE 2. Projection of the four selected hue orientation points onto the plane (a^*, b^*). The light gray region corresponds to the D65 gamut projection, the dark gray corresponds to its section by the plane $L^* = 50$ containing the selected points, and the same section of the sRGB [47] gamut is shown as the colored region.

This condition defines the parameters φ_2, φ_3, and ρ unambiguously, while the rotation angle φ_1 around the lightness axis is still undefined. To fix this parameter as well, let us require the hues of the saturated colors to be arranged approximately similar to CIELAB. Specifically, let us choose four equally saturated CIELAB points $C_l^{key} \subset C_l$ within the D65 gamut such that for each of them, the lightness is equal to half the maximum, and one color coordinate is equal to zero (see Fig. 2):

$$C_l^{key} \stackrel{\text{def}}{=} \left\{ \begin{bmatrix} 50 \\ -80 \\ 0 \end{bmatrix}, \begin{bmatrix} 50 \\ 80 \\ 0 \end{bmatrix}, \begin{bmatrix} 50 \\ 0 \\ -80 \end{bmatrix}, \begin{bmatrix} 50 \\ 0 \\ 80 \end{bmatrix} \right\}. \tag{15}$$

Then, we choose φ_1 such that the coordinates of the selected points in C_p differ from those in C_l as little as possible:

$$\varphi_1^{opt} = \arg\min_{\varphi_1} \sum_{\mathbf{c_l} \in C_l^{key}} \left\| \mathbf{c_l} - \mathrm{T_c}\Big(P(\boldsymbol{\varphi}, \rho, \boldsymbol{\mu})\mathrm{T_h}\big(\mathrm{L}^{-1}(\mathbf{c_l})\big)\Big) \right\|_2^2. \tag{16}$$

φ_1^{opt} can be found analytically by finding the optimal rotation [46].

Summarizing the above, we fully determine proLab as the transformation P constructed via the following steps:

- The optimal metric parameters $\boldsymbol{\mu}$ of the matrix M (12) are calculated according to the metric requirements.
- The scale and the lightness axis orientations are set to be the same as in CIELAB (14).
- The orientation of the color axes is determined according to (16).
- Normalization (9) is taken into account.

III. ADDITIONAL RESTRICTIONS ON THE PARAMETERS OF PROLAB

Now, let us define a subspace of the metric parameters, $\boldsymbol{\mu}$, over which the proLab color model can be interpreted meaningfully. First, we should note that not every projective transformation maps the original gamut into a bounded region. Let us require this natural property.

In the space C_x, let a plane given by the equation

$$\begin{bmatrix} p_{41} & p_{42} & p_{43} \end{bmatrix} \mathbf{c_x} + p_{44} = 0 \tag{17}$$

be called a horizon of the space C_p. On the horizon, the denominator of the rational transformation P vanishes. The gamut image in C_p is a bounded region if and only if the preimage of this gamut in C_x does not intersect with the horizon.

Now, let us formulate a simple sufficient condition under which the gamut is bounded in C_p. This condition does not require knowledge of the gamut shape. Note that the gamut of any light source in C_x always lies within an orthotropic rectangular box, the main diagonal of which connects vertices $\mathbf{0}$ and $\mathbf{c}_\mathbf{x}^*$. All eight vertices of this box can be listed as follows:

$$\mathrm{diag}\left(\mathbf{c}_\mathbf{x}^*\right)\mathbf{b}, \quad \mathbf{b} \in \{0, 1\}^3. \tag{18}$$

Taking into account the normalization (13), the condition on the gamut to be bounded in C_p can be written as the condition on all these vertices to be on the same side with regard to the horizon (17):

$$\begin{bmatrix} p_{41} & p_{42} & p_{43} \end{bmatrix} \mathrm{diag}\left(\mathbf{c}_\mathbf{x}^*\right)\mathbf{b} + 1 \geq 0, \quad \mathbf{b} \in \{0, 1\}^3. \tag{19}$$

Now, let us determine $\boldsymbol{\mu}$ under which this condition is fulfilled. From (8), (9) and (11), it follows that

$$\begin{aligned} \begin{bmatrix} \mu_6 & \mu_7 & \mu_8 \end{bmatrix} &= \begin{bmatrix} q_{41} & q_{42} & q_{43} \end{bmatrix} \\ &= \begin{bmatrix} p_{41} & p_{42} & p_{43} \end{bmatrix} \mathrm{diag}\left(\mathbf{c}_\mathbf{x}^*\right); \end{aligned} \tag{20}$$

thus, the condition (19) can be rewritten as

$$\begin{bmatrix} \mu_6 & \mu_7 & \mu_8 \end{bmatrix} \mathbf{b} + 1 \geq 0, \quad \mathbf{b} \in \{0, 1\}^3. \tag{21}$$

Note that for $\mathbf{b} = \mathbf{0}$, this condition is fulfilled for any $\boldsymbol{\mu}$.

Let us now introduce one more restriction. As with the coordinate L^* of the CIELAB space, we would like the first coordinate of proLab to represent the lightness. Therefore, we require the following:

$$\begin{aligned} \mathbf{0} \;\leq\; \mathbf{c_0}, \mathbf{c_1} \leq \mathbf{c}_\mathbf{x}^*, \quad \mathbf{c_1} - \mathbf{c_0} \in \mathbb{R}^3_{\geq 0} \\ \Longrightarrow \left(\mathrm{P}(\mathbf{c_1}) - \mathrm{P}(\mathbf{c_0})\right)^T \hat{\mathbf{e}}_\mathbf{L} \geq 0, \end{aligned} \tag{22}$$

where $\hat{\mathbf{e}}_\mathbf{L} \stackrel{\text{def}}{=} \begin{bmatrix} 1 & 0 & 0 \end{bmatrix}^T$ is the lightness unit vector (here and hereafter, we denote inequality for a vector as a system of inequalities restricting each of the coordinates). This restriction means that within the bounding box of the gamut, an increase in any coordinate in CIE XYZ should not lead to a decrease in the lightness coordinate in proLab.

Let us simplify the requirement (22). To do this, we consider a set of planes with equal lightness (the first coordinate) in proLab. In C_p, they can be expressed as

$$L^+ = L_s^+, \quad L^+ \stackrel{\text{def}}{=} \hat{\mathbf{e}}_{\mathbf{L}}{}^T \mathbf{c_p}. \tag{23}$$

Since P is projective, the preimage of the set of these planes forms a pencil of planes in C_x. At $0 \le L_s^+ \le 100$, the preimages of planes in C_x cross the rectangular box (18). Since we have already required the condition (19), we can consider the angle of the preimage rotation around the pencil axis to be a monotonic and continuous function of L_s^+ within the given range. Then, condition (22) is equivalent to the requirement that the coordinates of the normals should be of one sign. Since the sign of a normal's coordinates cannot be changed twice, we instead require all coordinates of the normals relative to the extreme planes (with equations $L^+ = 0$ and $L^+ = 100$) to be non-negative.

Let us define the restrictions on $\boldsymbol{\mu}$ under which this requirement is satisfied. First, we introduce another coordinate space C_b, which is constructed by the projective transformation B of the space C_x with a matrix $B \stackrel{\text{def}}{=} MN$:

$$\mathrm{B}(\mathbf{c_x}) \stackrel{\text{def}}{=} \mathrm{T_c}(MN\mathrm{T_h}(\mathbf{c_x})), \quad \mathbf{c_x} \in C_x, \quad \mathrm{B}(\mathbf{c_x}) \in C_b. \tag{24}$$

From (9) and (11), it follows that

$$P = R_1 R_2 R_3 Z B, \tag{25}$$

i.e., the space C_b is related to the space C_p through a similarity.

Let us denote the parameters of the plane given by the equation $\mathbf{l_\Phi}\mathrm{T_h}(\mathbf{c_\Phi}) = 0$ in an arbitrary color coordinate space C_Φ ($\mathbf{c_\Phi} \in C_\Phi$) as the vector $\mathbf{l_\Phi}$. According to the definition (24), the following relationship holds between parameters $\mathbf{l_x}$ of the planes in the C_x space and parameters $\mathbf{l_b}$ of the images of these planes in the C_b space:

$$\mathbf{l_x} = \mathbf{l_b} MN. \tag{26}$$

Thus, the restriction on the parameters of the line in the space C_b leads to the requirement of non-negative normal coordinates of this line image in the space C_x, which can be written as follows:

$$\mathbf{l_b} MN \ge \begin{bmatrix} 0 & 0 & 0 & -\infty \end{bmatrix}. \tag{27}$$

The matrix N is diagonal with positive elements; thus, the inequality can be simplified as follows:

$$\mathbf{l_b} M \ge \begin{bmatrix} 0 & 0 & 0 - & \infty \end{bmatrix}. \tag{28}$$

Now, let us apply this restriction to the planes $L^+ = 0$ and $L^+ = 100$ in C_p. For this, let us consider the white point image in the space C_b. Let us denote it as $\mathbf{c_b^*}$:

$$\mathbf{c_b^*} \stackrel{\text{def}}{=} \mathrm{B}\left(\mathbf{c_x^*}\right). \tag{29}$$

Since the planes of pencil $L^+ = L_s^+$ in the space C_p are orthogonal to the white point vector $\mathbf{c_p^*}$ in this space, their preimages are also orthogonal in the space C_b. This means that the parameters of the planes of this pencil in C_b are expressed as

$$\begin{bmatrix} \mathbf{c_b^*}{}^T & l_4\left(L_s^+\right) \end{bmatrix}, \tag{30}$$

where $l_4\left(L_s^+\right)$ denotes the dependency of the fourth coordinate of the plane parameters' vector on L_s^+.

The preimage of plane $L^+ = 0$ passes through $\mathbf{0}$, while the preimage of plane $L^+ = 100$ passes through the white point $\mathbf{c_b^*}$ in the space C_b. Hence, the parameters of the corresponding preimages are equal to $\begin{bmatrix} \mathbf{c_b^*}{}^T & 0 \end{bmatrix}$ and $\begin{bmatrix} \mathbf{c_b^*}{}^T & -\mathbf{c_b^*}{}^T\mathbf{c_b^*} \end{bmatrix}$, respectively.

Let us substitute these parameters into condition (28) and expand M in terms of definition (12):

$$\begin{bmatrix} \mathbf{c_b^*}{}^T & 0 \\ \mathbf{c_b^*}{}^T & -\mathbf{c_b^*}{}^T\mathbf{c_b^*} \end{bmatrix} \begin{bmatrix} \mu_1 & \mu_2 & \mu_3 \\ 0 & \mu_4 & \mu_5 \\ 0 & 0 & 1 \\ \mu_6 & \mu_7 & \mu_8 \end{bmatrix} \ge 0_{2,3}. \tag{31}$$

From definition (8), it follows that $N\mathrm{T_h}\left(\mathbf{c_x^*}\right) = \mathbf{1}$; thus,

$$\mathbf{c_b^*} = \mathrm{T_c}(MN\mathrm{T_h}\left(\mathbf{c_x^*}\right)) = \mathrm{T_c}(M\mathbf{1}). \tag{32}$$

Taking into account (12), we obtain

$$\mathbf{c_b^*} = \mathbf{m}/m, \quad \mathbf{m} = \begin{bmatrix} \mu_1 + \mu_2 + \mu_3 \\ \mu_4 + \mu_5 \\ 1 \end{bmatrix}, \quad m = \mu_6 + \mu_7 + \mu_8 + 1. \tag{33}$$

Due to condition (21) $m \ge 0$, the inequality (31) is equivalent to

$$\begin{bmatrix} m\mathbf{m}^T & 0 \\ m\mathbf{m}^T & -\mathbf{m}^T\mathbf{m} \end{bmatrix} \begin{bmatrix} \mu_1 & \mu_2 & \mu_3 \\ 0 & \mu_4 & \mu_5 \\ 0 & 0 & 1 \\ \mu_6 & \mu_7 & \mu_8 \end{bmatrix} \ge 0_{2,3}. \tag{34}$$

Finally, taking into account the 7 restrictions on $\boldsymbol{\mu}$ given in (19) and the 6 restrictions given in (34), we obtain 13 additional restrictions on the proLab parameters in the form

$$f_i(\boldsymbol{\mu}) \ge 0, \tag{35}$$

where $f_i(\boldsymbol{\mu})$ denotes polynomials of the third or smaller degree.

IV. PERCEPTUAL UNIFORMITY CRITERIA

In the region bounded by the above inequalities, let us find a vector $\boldsymbol{\mu}$ that maximizes the perceptual uniformity. The perceptual uniformity of a color coordinate space implies the accuracy of the perceptual color differences approximation by the Euclidean distances in this space. To quantify nonuniformity, the STRESS (STandardized REsidual Sum of Squares) criterion is usually employed: the higher the STRESS value is, the worse the uniformity [12], [48]–[50].

Let $\mathbf{a}$ denote the vector of color differences estimated in one approximation, and let $\mathbf{b}$ denote the vector of the same color differences estimated in some other approximation,

such that $\|\mathbf{a}\| \neq 0$ and $\|\mathbf{b}\| \neq 0$. The STRESS criterion for these two vectors is defined as follows:

$$\mathrm{STRESS}\,(\mathbf{a},\mathbf{b}) \stackrel{\mathrm{def}}{=} \frac{\|k\mathbf{a}-\mathbf{b}\|_2}{\|\mathbf{b}\|_2}, \quad k=\frac{(\mathbf{a},\mathbf{b})}{\|\mathbf{a}\|_2^2}, \tag{36}$$

and it is easy to see that the STRESS criterion is equal to the absolute value of the sine of the angle between $\mathbf{a}$ and $\mathbf{b}$:

$$\mathrm{STRESS}\,(\mathbf{a},\mathbf{b}) = \sqrt{1-\frac{(\mathbf{a},\mathbf{b})^2}{\|\mathbf{a}\|_2^2\,\|\mathbf{b}\|_2^2}} = \left|\sin\widehat{\mathbf{ab}}\right|. \tag{37}$$

This criterion is symmetric and invariant to scaling by either of the two compared estimations:

$$\mathrm{STRESS}\,(k\mathbf{a},\mathbf{b}) = \mathrm{STRESS}\,(\mathbf{b},\mathbf{a}), \quad k\neq 0. \tag{38}$$

Hence, fixing the color coordinate scale as given by the condition (14) does not affect the correspondence evaluation via the STRESS criterion.

This criterion is also invariant to equal permutations of color difference vector components:

$$\mathrm{STRESS}\,(M_\pi\mathbf{a},M_\pi\mathbf{b}) = \mathrm{STRESS}\,(\mathbf{a},\mathbf{b}), \tag{39}$$

where M_π is an arbitrary permutation matrix. Thus, STRESS can be defined on a multiset of ordered difference pairs. Let us consider $\omega = \{(a_i,b_i) \mid 1 \leq i \leq n\}$, $\mathbf{a},\mathbf{b} \in \mathbb{R}^n$ as a finite sample of ordered pairs of real numbers. The STRESS criterion for this sample is defined in an obvious way:

$$\mathrm{STRESS}\,(\omega) \stackrel{\mathrm{def}}{=} \mathrm{STRESS}\,(\mathbf{a},\mathbf{b}). \tag{40}$$

The STRESS value can be significantly dependent on the distribution of the measured samples. The values measured in perceptual experiments (as in [12]) or obtained using color difference formulas (as in [51], [52]) are used as a reference. The disadvantage of the first approach is the fixed and limited number of samples (3657 color pairs among all datasets as of 2001 [11]); hence, a question arises regarding the space coverage and the sample distribution balance. The disadvantage of the second approach is the additional approximation error. In this work, we use the second approach, employing the CIEDE2000 formula [10], [11] as the reference.

The considered alternative has direct analogies to machine learning. The experimental data represent the initial training sample. The target color space can be considered as a representation space [53], [54] with a specific set of desired properties. The more complex CIEDE2000 model fitted to the original experimental data can be used as a training sample generator instead of source data. This can be considered as knowledge distillation [55].

Following [52], let us construct the pairs from the color vectors uniformly distributed within the light source gamut in the CIELAB space. However, unlike [52], we do not place an upper bound on the color difference in each pair, as we do not want to be limited to the analysis of small differences only.

Let us denote the D65 gamut as $G \subset C_l$ and the uniform sample from this gamut as G_n ($G_n \subset G, |G_n| = n$). We similarly denote the uniform sample of the gamut's color pairs as G_n^2 ($G_n^2 \subset G^2 \subset C_l^2, |G_n^2| = n$). Finally, we denote the reference CIEDE2000 color difference of the color pair $p \in C_l^2$ as $\Delta\mathrm{E}^*_{00}(p)$ as Φ – the transformation into the considered space C_Φ from C_x, and as Φ_L – the same from C_l ($\Phi_\mathrm{L} = \Phi \circ \mathrm{L}^{-1}$), where $\circ$ is the composition of transformations. Then, the criterion of nonuniformity of the color coordinate space C_Φ over the sample G_n^2 can be written as follows:

$$\mathrm{U}[\Phi, G_n^2] \stackrel{\mathrm{def}}{=} \mathrm{STRESS}(\omega),$$
$$\omega = \left\{\left(\|\Phi_\mathrm{L}(\mathbf{c_a})-\Phi_\mathrm{L}(\mathbf{c_b})\|_2\,,\,\Delta\mathrm{E}^*_{00}(p)\right) \mid p=(\mathbf{c_a},\mathbf{c_b}) \in G_n^2\right\}. \tag{41}$$

V. OPTIMAL PROLAB PARAMETERS

To obtain proLab parameters according to all the aforesaid, we performed the following steps:

1) We computed the grid of points on the surface of the D65 gamut G using the method described by V. Maksimov in [56]. 2D triangulation was constructed for these points, which allowed G to be approximated by a polyhedron with $\sim$ 20 000 faces. Since G is a convex set, in further analysis, we used a system of linear inequalities to check whether the points were inside the gamut G. Each of the inequalities verifies the positions of points relative to one of the faces.
2) The sample G_{2n_1} consisting of $2n_1$ independent and identically distributed CIELAB colors that belonged to the gamut G was generated, where $n_1 = 10\,000$. By division of the sample G_{2n_1} into n_1 pairs, a sample of pairs $G_{n_1}^2$ was formed.
3) To determine the metric parameters $\boldsymbol{\mu}^{opt}$, we solved the optimization problem with penalty functions [57]:

$$\boldsymbol{\mu}^{opt} = \arg\min_{\boldsymbol{\mu}\in\mathbb{R}^8} \mathrm{U}[C_m(\boldsymbol{\mu}), G_{n_1}^2] + \sigma\sum_{i=1}^{14}\max(0,-f_i(\boldsymbol{\mu}))^2, \tag{42}$$

where σ is a parameter of the penalty function method, $\mathbf{f}$ is a vector of functions corresponding to the conditions given above: $f_1 = |M| = \mu_1\mu_4$ – to the condition (12), $\{f_2,\ldots,f_8\}$ – to 7 nontrivial linear conditions (21), and $\{f_9,\ldots,f_{14}\}$ – to 6 cubic conditions (34). To calculate the criterion U, we obtained values of $\Delta\mathrm{E}^*_{00}$ according to the procedures described in [58]. Problem (42) was solved numerically via multistart sequential quadratic programming [59], [60]. As a result, we obtained the following matrix of metric parameters (12):

$$M = \begin{bmatrix} 2.1591 & -1.7823 & -0.0713 & 0 \\ 0 & 2.0865 & 0.2103 & 0 \\ 0 & 0 & 1 & 0 \\ 0.7554 & 3.8666 & 1.6739 & 1 \end{bmatrix}. \tag{43}$$

4) To fully determine matrix Q (11), we found the parameters $\boldsymbol{\varphi}$ and ρ analytically (see Section II). As a result, the following matrix Q was formed:

$$Q = \begin{bmatrix} 75.54 & 486.66 & 167.39 & 0 \\ 617.72 & -595.45 & -22.27 & 0 \\ 48.34 & 194.94 & -243.28 & 0 \\ 0.7554 & 3.8666 & 1.6739 & 1 \end{bmatrix}. \quad (44)$$

Thus, for a D65 light source with coordinates $\mathbf{c}_{\mathbf{x}}^{*} = \begin{bmatrix} 0.95047 & 1 & 1.08883 \end{bmatrix}^T$ [61], we can obtain the following proLab parameters:

$$P = \begin{bmatrix} 79.477 & 486.66 & 153.73 & 0 \\ 649.91 & -595.45 & -20.453 & 0 \\ 50.859 & 194.94 & -223.43 & 0 \\ 0.7948 & 3.8666 & 1.5373 & 1 \end{bmatrix}. \quad (45)$$

VI. CRITERION OF NOISE HETEROSCEDASTICITY

As we mentioned in the introduction, the color values captured by a camera are always noisy. As a rule, statistical methods for color distribution analysis consider the image noise as homoscedastic. To validate this, let us construct a criterion to estimate the heteroscedasticity of color vector noise in the space of color coordinates.

Let us consider the color coordinate space C_Φ with the known transformation $\Phi : C_x \to C_\Phi$. We assume that at each point $\mathbf{c_x} \in C_x$, the noise is approximately additive, with zero mean and a known covariance matrix $\Sigma_x(\mathbf{c_x})$. Then, the covariance of the noise in the C_Φ space could be roughly expressed as follows:

$$\Sigma_\Phi(\mathbf{c_\Phi}) = J_\Phi(\mathbf{c_x})\, \Sigma_x\,(\mathbf{c_x})\, J_\Phi^T(\mathbf{c_x}), \quad \mathbf{c_x} = \Phi^{-1}\,(\mathbf{c_\Phi})\,, \quad (46)$$

where J_Φ is the Jacobian matrix of the transformation Φ.

We consider the noise to be homoscedastic if all three eigenvalues of its covariance matrix are equal throughout the gamut. Then, on the color sample G_n, we can estimate the hardware noise heteroscedasticity in the C_Φ space as follows:

$$\begin{aligned} &\mathrm{H}[\Phi, G_n] \\ &\quad \stackrel{\text{def}}{=} \mathrm{STRESS}(\omega), \\ &\omega = \left\{ \left(\lambda_i^{1/2} \left[\Sigma_\Phi(\Phi_{\mathrm{L}}(\mathbf{c_l})) \right], 1 \right) \mid \mathbf{c_l} \in G_n, 1 \le i \le 3 \right\}, \end{aligned} \quad (47)$$

where $\lambda_i[A]$ is the i-th eigenvalue of a matrix A.

VII. NOISE PARAMETERS IN THE SENSOR COLOR SPACE AND OTHER SPACES

Let us construct a noise model for the original sensor color space. A very simple model of the output values for a single-channel image, which nevertheless agrees well with the experiments, was proposed by Jähne in [37]:

$$s = g\,n + \varepsilon, \quad n \sim \mathrm{Pois}(s_0), \quad \mathbb{E}(\varepsilon) = 0, \quad (48)$$

where s is a random sensor response, g is a gain coefficient, n is a random number of registered electrons, s_0 is the expected sensor response value at $g = 1$, and ε is additive noise independent of the sensor irradiance.

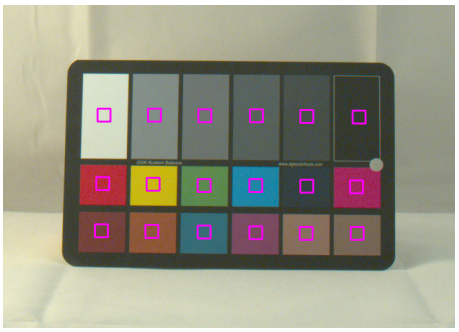

FIGURE 3. Colorchecker captured using Canon 5D Mark III camera. The areas used for the estimation of the sensor response mean and variance are marked with violet rectangles.

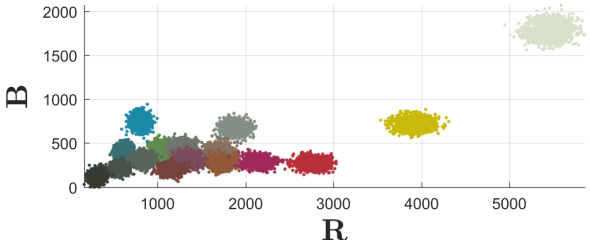

FIGURE 4. Sensor responses for each patch of the color chart.

According to (48), the relationship between the mean and variance of the output values is linear:

$$\mathbb{V}(s) = g\,\mathbb{E}(s) + \mathbb{V}(\varepsilon). \quad (49)$$

To verify this model, let us take the MLSDCR (Multiple Light Source Dataset for Colour Research) dataset [62], which was captured using a Canon 5D Mark III camera. Among various scenes, the MLSDCR contains raw images of the colorchecker (see Fig. 3); parameters of the calibration transformation from the camera color space into the standard observer color space (in sRGB [47] coordinates) are also provided.

Let us estimate the noise parameters for each patch (uniformly colored area) of the color chart. The measurement accuracy of the color calibration experiments may be limited by irradiance nonuniformity [18]. Thus, we need to track the irradiance uniformity – but only inside each patch, not between them. To reduce the impact of irradiance nonuniformity, we take a small central area of 42×42 Bayer mosaic pixels (see Fig. 3) for each patch of the color chart. We also take into account that different mosaic elements can have different noise parameters. In the Canon 5D Mark III camera, a standard (RGGB) Bayer mosaic is used, so for each of the 18 patches, we form a sample S_i ($1 \le i \le 72$) of sensor responses for uniform irradiance. Joint histograms of color coordinates through the sample elements demonstrate significant noise heteroscedasticity (see Fig. 4).

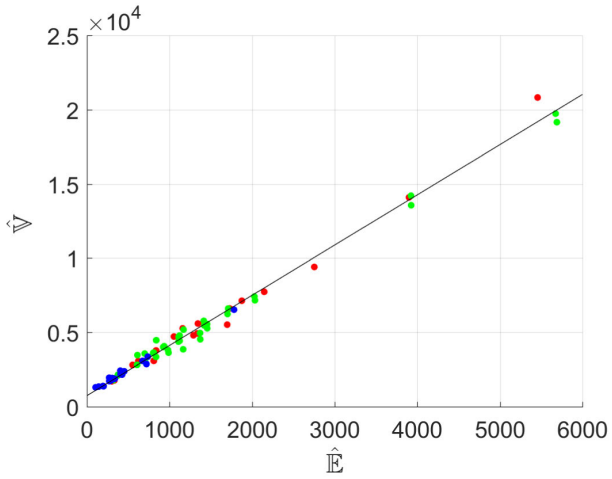

FIGURE 5. Linear dependency of the sensor response variance on its average sample value. Colors of points correspond to the conventional names of the sensor channels.

Let us estimate the mean and variance of the sensor responses for each element of S_i:

$$\hat{\mathbb{E}}_i = \overline{S_i}, \quad \hat{\mathbb{V}}_i = \overline{(S_i - \overline{S_i})^2}, \quad 1 \le i \le 72. \tag{50}$$

Using principal component analysis, we estimate parameters of the model given in (49):

$$\hat{g} = 3.38, \quad \hat{\mathbb{V}}(\varepsilon) = 744. \tag{51}$$

The relationship between the sample estimations $\hat{\mathbb{E}}(s)$ and $\hat{\mathbb{V}}(s)$ can be approximated with good reliability by linear dependency (see Fig. 5). Thus, we estimate the variance in the Bayer mosaic value captured using the Canon 5D Mark III camera as follows:

$$\hat{\mathbb{V}}(s) = 3.38\, s + 744. \tag{52}$$

Let us consider the transformation into the C_x space. We use the transformation described in [62], from which the experimental data were obtained. In this work, the sensor color coordinate space is obtained via the simplest debayering algorithm, which employs an averaging of two mosaic G-elements and aggregates the average with a single R- and a single B-element. Let us call this space 'deviceRGB' and denote it as C_d. Taking into account the noise model described above (52), the covariance matrix of the noise in C_d could be written as

$$\Sigma_d(\mathbf{c_d}) = \operatorname{diag}\left(\begin{bmatrix}1 & 1/2 & 1\end{bmatrix}\right)(3.38\operatorname{diag}(\mathbf{c_d}) + 744\, I_3), \quad \mathbf{c_d} \in C_d. \tag{53}$$

The transformation matrix from deviceRGB to the standard observer linRGB is described in [62]:

$$D_1 = \frac{0.03}{2^{16}}\begin{bmatrix}41.93 & -2.08 & -37.24\\ -14.32 & 39.13 & 10.79\\ -0.02 & -35.39 & 185.52\end{bmatrix}. \tag{54}$$

Considering that the transformation from linRGB to CIE XYZ is linear [47] and given by the matrix

$$D_2 \stackrel{\text{def}}{=} \begin{bmatrix}0.4125 & 0.3576 & 0.1804\\ 0.2127 & 0.7152 & 0.0722\\ 0.0193 & 0.1192 & 0.9503\end{bmatrix}, \tag{55}$$

we obtain the following transformation matrix from C_d to C_x:

$$D^{-1} = D_2$$
$$D_1 = 10^{-6}\begin{bmatrix}5.5711 & 3.0892 & 10.0585\\ -0.6066 & 11.4383 & 6.0363\\ -0.4189 & -13.2786 & 80.9631\end{bmatrix}. \tag{56}$$

The sensor noise covariance matrix in the CIE XYZ space is equal to

$$\Sigma_x(\mathbf{c_x}) = D^{-1}\,\Sigma_d(D\mathbf{c_x})\,D^{-T}, \quad \mathbf{c_x} \in C_x. \tag{57}$$

By substituting the parameter values from (53) and (56) into (57), we obtain the numerical color noise model for our camera in the C_x space.

VIII. COMPARING THE PERFORMANCE OF PROLAB WITH THAT OF OTHER PERCEPTUALLY UNIFORM COLOR SPACES

We estimate the perceptual nonuniformity further according to the criterion (41): $\mathrm{U_T}[\Phi] \stackrel{\text{def}}{=} \mathrm{U}[\Phi, G^2_{n_2}]$, where Φ is the transformation from CIE XYZ by which the system is defined. To do this, we form an independent test sample $G^2_{n_2}$ of $n_2 = 100\,000$ pairs, according to the method described in Section V.

Let us also construct a test G_{n_2} of individual colors to estimate the noise heteroscedasticity. In doing so, we require all of the color vectors not only to belong to the D65 source gamut but also to be reproducible by the camera – i.e., we require each component of the color vectors to be non-negative in deviceRGB space:

$$\mathbf{c_l} \in G_{n_2} \Longrightarrow D\mathrm{L}^{-1}(\mathbf{c_l}) \ge 0. \tag{58}$$

We perform uniform sampling G_{n_2} from a reproducible subarea of the gamut and estimate the heteroscedasticity according to the criterion (47): $\mathrm{H_T}[\Phi] \stackrel{\text{def}}{=} \mathrm{H}[\Phi, G_{n_2}]$. To calculate $\mathrm{H_T}[\Phi]$, we need to use the noise covariance matrix $\Sigma_\Phi(\mathbf{c_\Phi})$, which we obtain using approximation (46) along with the color noise model (57) in the C_x space.

The proposed color coordinate space was further compared with the following ones:

- CIE XYZ [2] – basic color coordinate system of the standard observer;
- CIE xyY [2] – system with distinct chromaticity coordinates;
- LMS [3] – coordinate system that models linearized human cone responses;
- sRGB [47] – color coordinates used to represent colors on displays and printers (most photos and videos are coded with these coordinates);

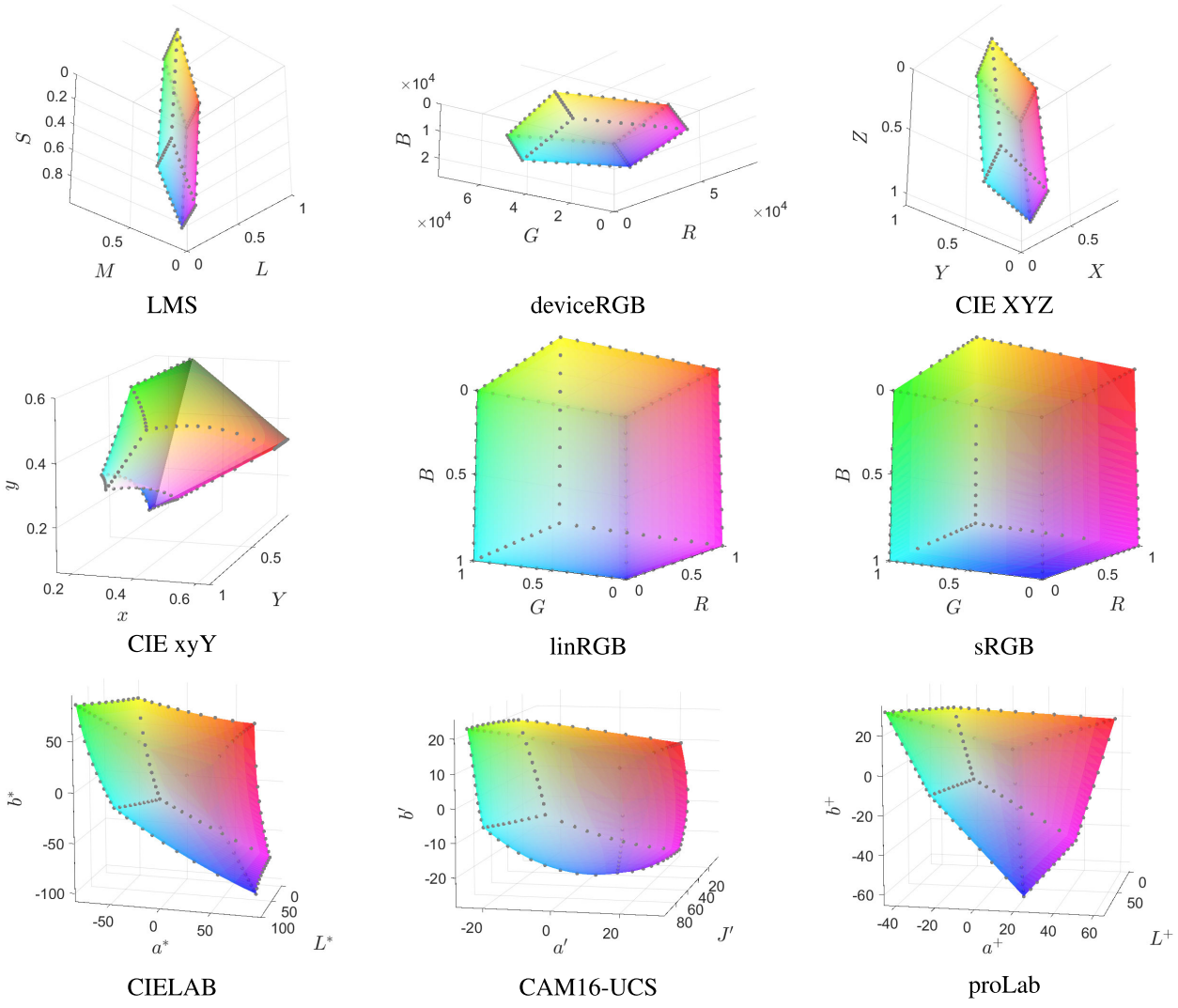

FIGURE 6. The sRGB gamut in various color coordinate spaces.

- linRGB [47] – intermediate (without gamma correction) representation of reproduced colors linearly related to CIE XYZ;
- CIELAB [8] – widely spread perceptually uniform color coordinates;
- CAM16-UCS [13] – the most perceptually uniform coordinate system at the time of writing.

We compare these color spaces and linear color coordinates of the camera sensor with proLab via the criteria U_T and H_T. Table 1 demonstrates the results of a quantitative comparison using U_T and H_T. We also specify whether each of the color coordinate systems preserves linearity of the color manifolds. ProLab preserves lines by its construction as well as linear coordinate systems; only CIE xyY has a nontrivial classification by collineation, since it keeps lines passing through $\mathbf{0}$ as lines. The rest of the color coordinate systems do not keep even the central pencil linear. Regarding perceptual uniformity, proLab is inferior to CAM16-UCS – the modern and currently most accurate space – but it is significantly superior to the common CIELAB uniform space. Our experiments also show that proLab is inferior in terms of noise homoscedasticity only to the deviceRGB space, the properties of which vary significantly from camera to camera.

TABLE 1. Performance of the color coordinate systems. Bold underlined font indicates the best criteria results; bold only – second best.

C_Φ space	**Collineation**	$U_T[\Phi]$	$H_T[\Phi]$
LMS	**Yes**	0.475	0.720
deviceRGB	**Yes**	0.474	**0.470**
CIE XYZ	**Yes**	0.479	0.722
CIE xyY	**Central pencil**	0.296	0.822
linRGB	**Yes**	0.381	0.607
sRGB	No	0.316	0.830
CIELAB	No	0.259	0.848
CAM16-UCS	No	**0.177**	0.696
proLab	**Yes**	**0.209**	**0.565**

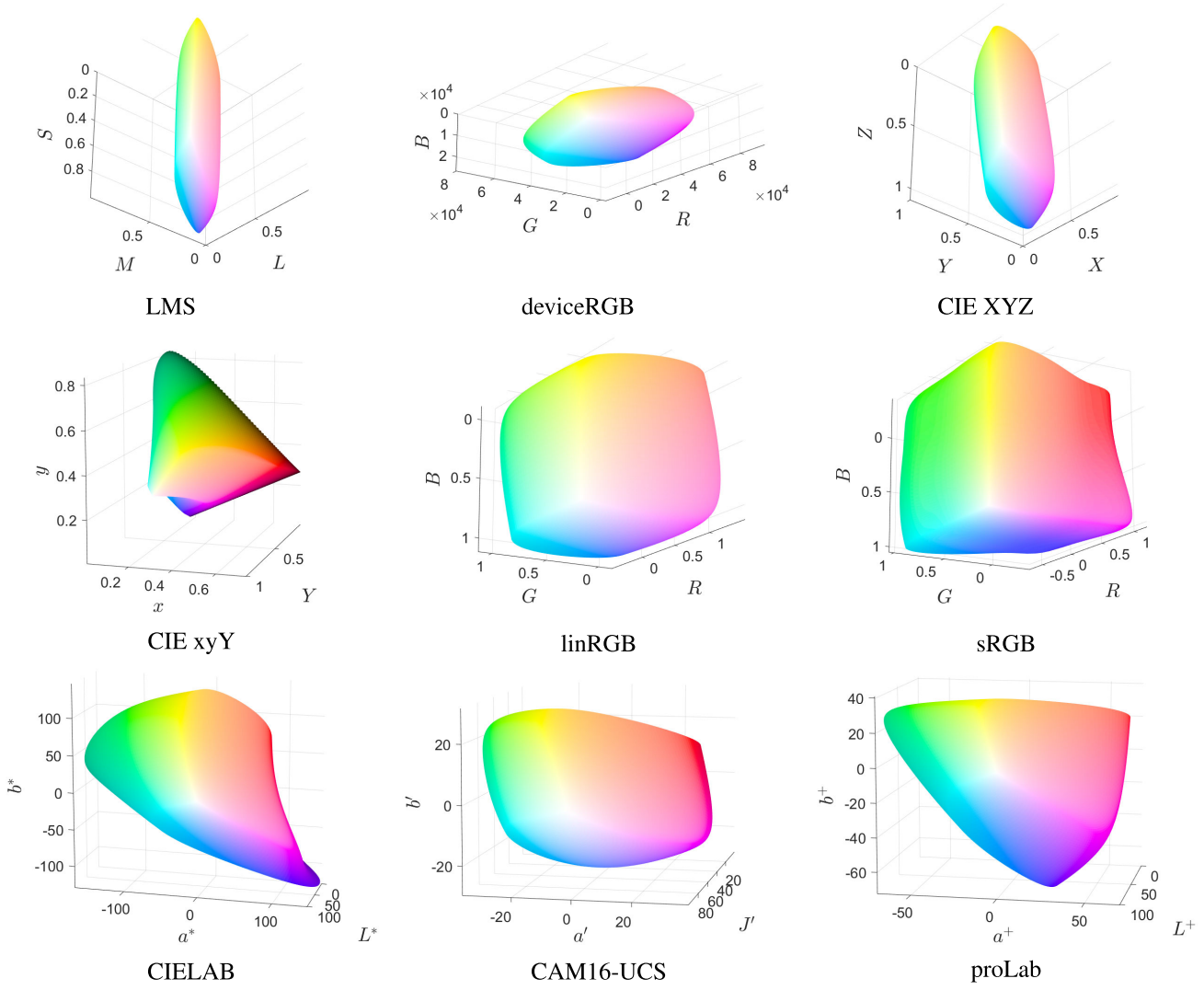

FIGURE 7. D65 light source gamut in various color coordinate spaces.

Let us employ various visualizations to analyze the differences between the color coordinate spaces more clearly. Figures 6 and 7 show the sRGB display gamut in various color coordinate spaces. The saturation of colors used for the visualization was decreased significantly in this illustration due to color coverage restrictions. ProLab preserves the shape of the sRGB gamut as a hexahedron. Another advantage is that proLab, unlike CIELAB, keeps the convexity of the gamut.

In Fig. 8, we show the color nonuniformity over the chromaticity diagram with MacAdam ellipses [63], which are just noticeable color differences (JND) scaled up 10 times; they were originally defined in CIE xyY. To plot them for each given color space C_Φ, we use a linear approximation of the transformation Φ around the ellipse centers.

In Fig. 9, we visualize color nonuniformities with joint distributions of the Euclidean distances ΔE_Φ and CIEDE2000 color differences ΔE^*_{00} over test sample $G^2_{n_2}$ for each color coordinate space. On these scatter plots, the thinner the cluster along the line passing through $\mathbf{0}$, the more perceptually uniform the color coordinate space is. The CAM16-UCS and proLab joint distributions have significantly better shapes than those of the other color coordinate spaces, but proLab is inferior to CAM16-UCS in the middle-range distances. Note that in a region of large Euclidean distances, CAM16-UCS has two distinctly different loci, which means there is significant nonuniformity in this range. Strongly decorrelated regions similar in location and shape are observed in proLab and CIELAB; however, for CIELAB, the region is larger and deviates more and farther from the main locus.

To provide a detailed visualization of the noise heteroscedasticity, we plot charts similar to the MacAdam ellipses (Fig. 10). For a set of colors from the sRGB gamut,

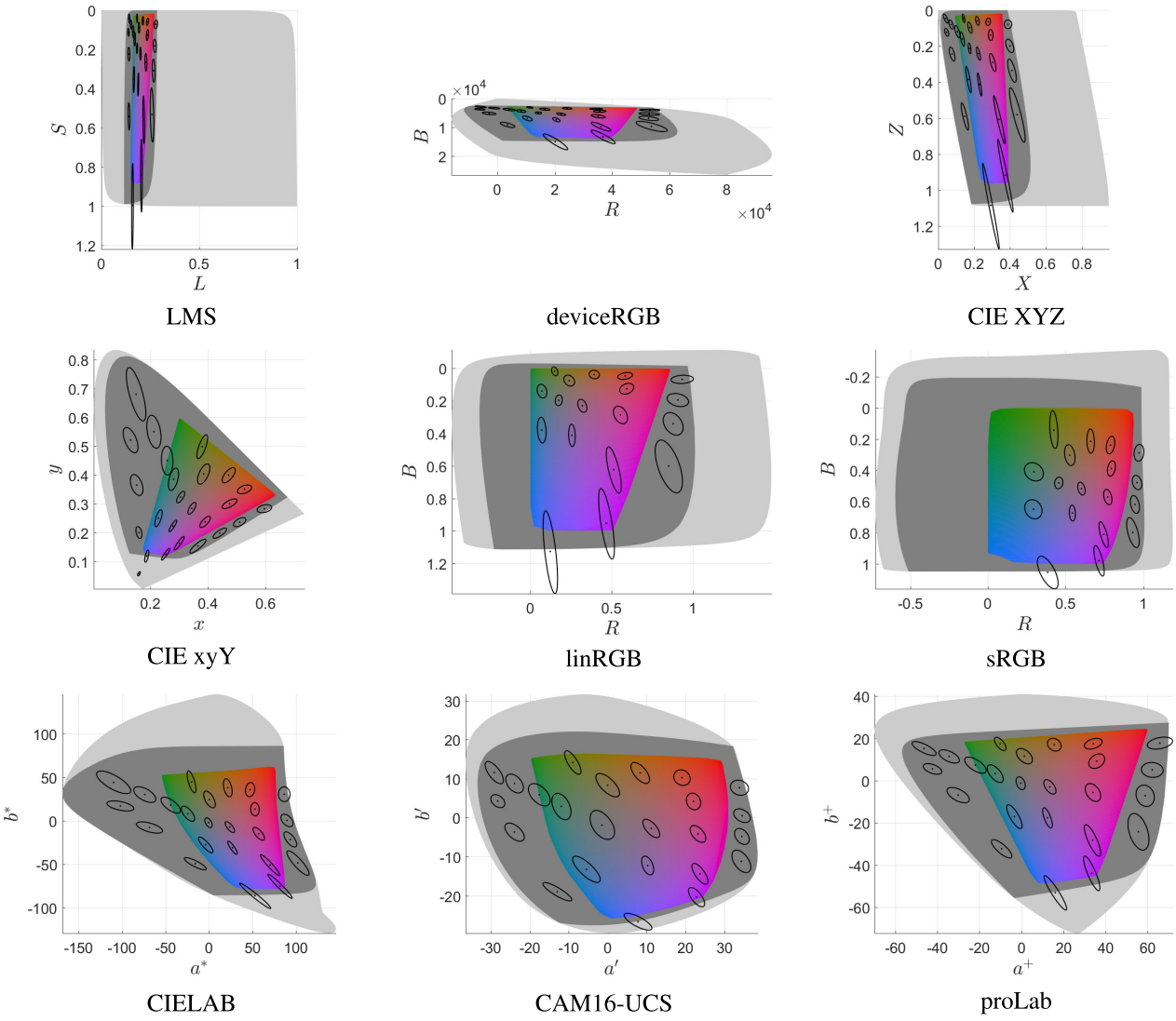

FIGURE 8. MacAdam ellipses for $L^* = 50$. The sRGB display gamut cross-section is shown in rainbow colors; the D65 light source gamut cross-section and projection are shown in dark gray and light gray, respectively.

we model the noise distributions of measurements according to the parameters of model (52). Each distribution is projected onto the given color coordinate space and visualized with its averaged color. The 3D structure of the noise parameters is visualized by plotting the lighter colors over the darker ones.

IX. POSSIBLE APPLICATIONS OF PROLAB

The useful properties of proLab are its collinearity, uniformity, and computational efficiency. These properties are key to its applications, which we consider further.

A. GAMUT COVERAGE ANALYSIS

The range of colors reproduced by a device is referred to as a gamut of that device. Two nonblack colors have matching chromaticity if and only if their linear coordinates are proportional: $\mathbf{c}_1 \sim \mathbf{c}_2$. A projection of the gamut (except the black color) on a plane is called a chromaticity diagram of this gamut if the matching colors are projected to the same point on the plane and the nonmatching colors are mapped to different points.

The chromaticity diagrams are usually plotted via central projection on a plane in one of the linear color coordinate systems. This plotting yields a polygon image of a gamut on the corresponding chromaticity diagram in color-reproducing devices, which are based on the principle of mixing radiation of fixed chromaticities and variable brightness. This principle is employed in most projectors and self-luminous displays. The number of vertices of the polygon depends on the number of color channels. The gamut is described by a triangle, as there are usually three channels.

The left side of Fig. 11 shows a standard chromaticity diagram in color coordinates (x, y) [2] for the sRGB gamut [47] (multicolor triangle) and the Adobe RGB 1998 gamut [64] (outlined by a black triangle). The gray area corresponds to the color triangle, i.e., all chromaticities of colors, perceived by a standard observer.

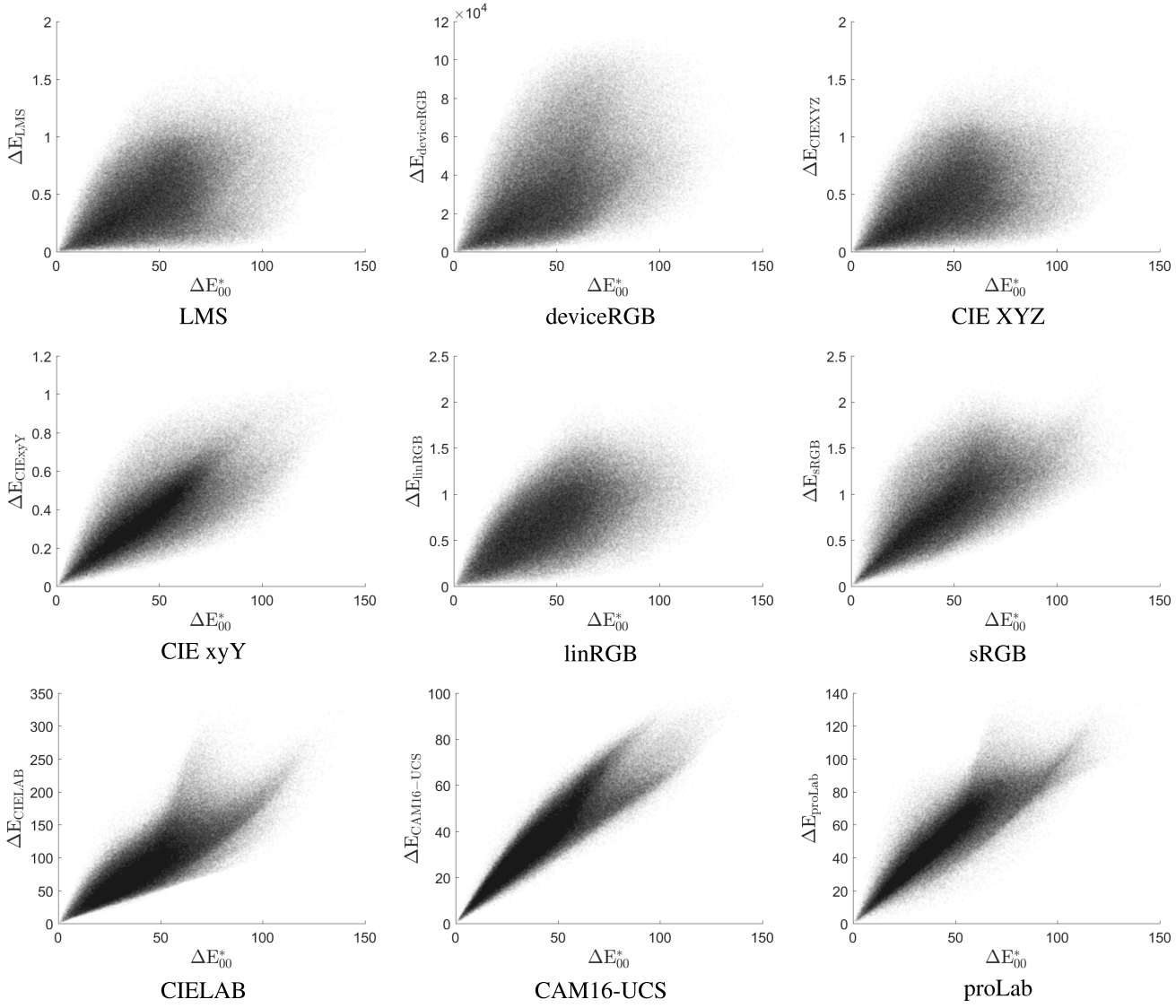

FIGURE 9. Joint distributions of CIEDE2000 color differences ΔE^*_{00} and Euclidean distances ΔE_Φ for various color coordinate systems.

The following conclusions can be drawn from this well-known illustration: (a) the color gamut of sRGB devices does not allow displaying a significant area of saturated cyan and especially green colors, and (b) the incremental color gamut of Adobe RGB relative to sRGB is quite significant. Note that these conclusions are groundless, since they are based on the implicit assumption that the elements of length and area are equivalent at different points of the chromaticity diagram. This property is met (at least approximately) only in uniform color coordinate systems.

To verify our conclusions, we consider CAM16-UCS, a color coordinate system with high uniformity. Because of the nonprojectivity of this space, sets of colors with the same chromaticities are not represented by straight lines. The easiest and most natural way to introduce chromatic coordinates is as follows: $a'_{xy} = a'(t\mathbf{c_x})$, $b'_{xy} = b'(t\mathbf{c_x})$, where J', a', b' are color coordinates in CAM16-UCS, $\mathbf{c_x} = \begin{bmatrix} x & y & 1-x-y \end{bmatrix}^T \in C_x$, and the scalar $t > 0$ is such that $J'(t\mathbf{c_x}) = 50$. The chromaticity diagram in terms of these coordinates for each considered gamut is shown in Fig. 11 in the center. It is clear that the color gamut of Adobe RGB 1998 is not as superior to sRGB as previously thought. More importantly, the green color segment, where the two gamuts differ, is not the most significant area not covered by sRGB. After switching to a uniform color coordinate system, it becomes obvious that standard displays do not represent magenta colors in a large saturation range, which previously was not possible to learn from the classical diagram. On the other hand, the CAM16-UCS space chromaticity diagram differs from the classical one in its complex shape. This makes both the visual analysis and formal numerical comparison of areas difficult.

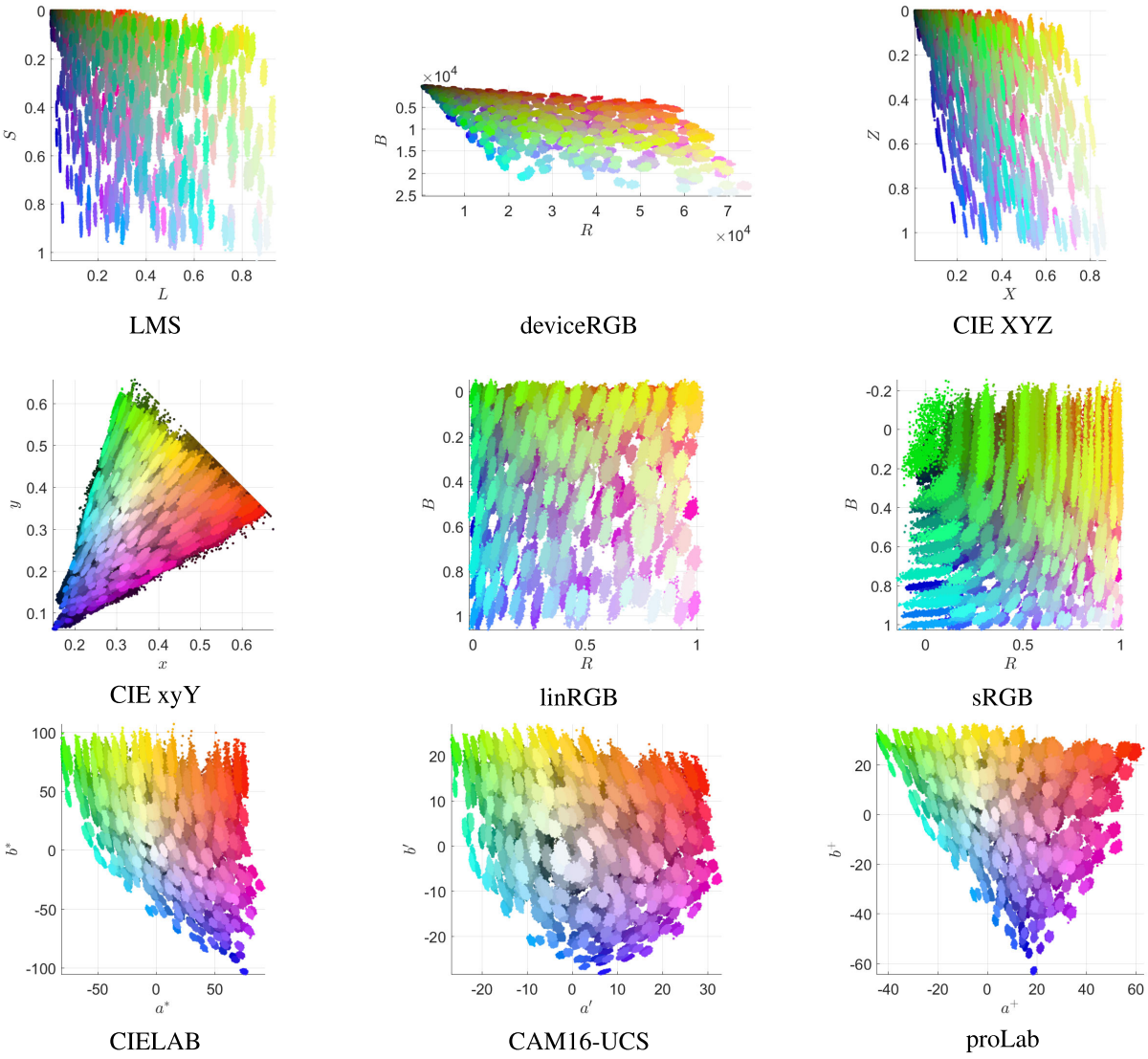

FIGURE 10. Visualization of sensor noise in different color coordinate spaces within the sRGB display gamut. Each individual cloud is a projection of a certain measured color sample for which the noise is described by the Jähne model.

In the proLab space, thanks to the collinearity property, the color coordinates can be introduced in the standard way: $(a^+/L^+, b^+/L^+)$. The chromaticity diagram in these coordinates is shown in Fig. 11 on the right. The proLab space, unlike CAM16-UCS, retains the convexity of the color triangle, and the images of gamuts remain geometric triangles, making proLab much more user friendly. The area ratios in the proLab chromaticity chart are adequate, unlike those in the standard chromaticity chart.

The gamut coverage can also be determined via its volume. For example, [65], [66] employ the gamut volume in the CIE XYZ space as a quantitative measure of color coverage, and [67] employs it in the CUELUV and CIELAB spaces. At the same time, it makes little sense to use the CIE XYZ space for these purposes because it is nonuniform, and using CUELUV, CIELAB and other known uniform color spaces is inconvenient because the gamuts there have complex shapes for calculating the volume (Fig. 6), which is especially important when attempting to maximize the volume of a gamut [66]. Both of these disadvantages can be overcome when using the proLab space.

B. COLOR UNMIXING FRAMEWORK

As we mentioned above, proLab is designed for use in image processing algorithms based on the analysis of affine color manifolds. These algorithms have been proposed in recent years, in particular, to solve the following problems:

- chroma keying (allocation of a single-color background when shooting with augmented reality technology) [68];
- soft color segmentation (segmentation into single-color interpenetrating areas) [69], [70];
- image-based rendering in the presence of reflective surfaces (3D modeling of real glossy objects under new observation conditions) [71], [72];

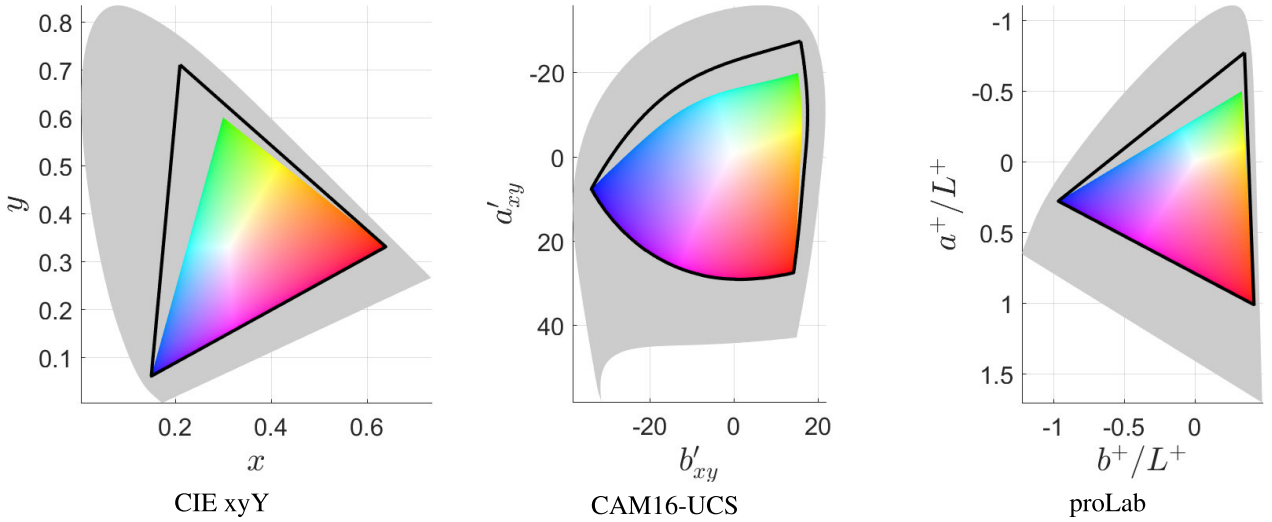

FIGURE 11. Chromaticity diagrams of the D65 light source gamut in different color spaces. Colors represent the sRGB color gamut; black outline represents the Adobe RGB 1998 gamut. The gray background corresponds to the remaining colors of the color cone.

- illumination decomposition for material recoloring (recoloring of real objects, taking into account inter-reflexes) [73].

In all the above papers, the proposed algorithms are based on the color unmixing framework, where it is assumed that each pixel of an image can be decomposed into a weighted sum of several color vectors, the ''base'' (underlying) colors, present in the image. This model is in perfect agreement with the linear physical theory of image formation described in I-D. In the color unmixing framework, the decomposition coefficients are not subject to any analytical model but are calculated empirically. Hence, the projective transformation (as opposed to the arbitrary nonlinear one) of the color space does not violate the color unmixing framework assumptions. It is important that in all of the discussed applications, the goal is to produce images that are realistic in terms of human perception. However, the authors minimize decomposition errors in linear RGB, which is perceptually nonuniform. Minimizing errors in proLab could improve the perceptual quality while keeping the algorithm the same.

The situation with chroma keying is more complicated. What matters here is how homoscedastic the color deviations of the real scene background from the ideal model of the green background are. With heteroscedastic outliers, it is difficult to choose a threshold separating objects from the background. Let us consider a ''naive'' chroma keying algorithm. Suppose we know an area that fully belongs to the background (the yellow rectangular outline in Fig. 12 on the left). Let the background color distribution be of the rank of 2: up to noise and distortion accuracy, it lies in some plane of the color coordinate space. Let us define the parameters of this plane as follows. The plane passes through the center of mass of the considered region's color distribution. The plane is perpendicular to the eigenvector of the covariance matrix of this distribution. This eigenvector corresponds to the smallest eigenvalue V_{min}. All colors that are within no less than $5\sqrt{V_{min}}$ from the selected plane are considered background colors. The result of this algorithm is shown in Fig. 12. It demonstrates that the Euclidean metric of proLab allows separating the object from the background much more accurately while using the simple threshold method.

C. TELEVISION AND CINEMA

The work in [74] introduces 8 criteria that the color coordinate system must meet to fulfill the requirements of ITU-R Recommendation BT.2020 for modern television devices. These criteria include (i) Local Uniformity, (ii) Global Uniformity, (iii) High Dynamic Range, (iv) Wide Color Gamut, (v) Hue Linearity, (vi) Neutral Point Convergence, (vii) Neutral Point (Locus) Error, and (viii) Computational Cost.

The first two criteria concern the isotropy and uniformity of the color coordinate space measured by the STRESS criterion. These properties of proLab are discussed in detail in the main section and are quite consistent with other equal-contrast color coordinate systems. Criteria (v)-(vii) for proLab are met with absolute accuracy (due to its collinearity-preserving property), which is advantageous compared with other equal-contrast systems applied to this problem. Whether proLab meets the High Dynamic Range and Wide Color Gamut criteria is a question for a separate study. However, it should be noted that according to [74], CIELAB meets these criteria sufficiently, and the color gamut of proLab is not inferior to that of CIELAB.

We already mentioned that computational simplicity is another important feature of proLab. In the examples discussed earlier, computational simplicity was a desirable but not the main aspect. In this case, however, the Computational Cost criterion is explicitly stated along with Equal Contrast. This is not surprising, since the video stream processing of modern television devices is extremely complex,

FIGURE 12. The performance of the "naive" chroma keying algorithm in the linRGB and proLab color spaces for the image from the dataset published in [68].

computational resources are limited, and the processing takes place in real time. Among the considered uniform spaces, CIELAB is the leader in computational simplicity. ICaCb and zICaCb result in slightly worse performance and have a computational structure close to that of proLab. This allows us to compare against them theoretically, avoiding the danger of incorrect conclusions due to an inconsistent implementation quality. Transitioning to these systems requires applying the linear 3D transformation twice, which gives 18 multiplication operations versus 16 for proLab. In addition to the multiplication operations, the transition to proLab requires three division operations versus three applications of the nonlinear transition function in ICaCb family systems. Thus, the computational complexity of the considered systems is almost consistent, while that of CAM16-UCS is approximately 4 times worse [74].

To sum up, proLab should be considered as one of the color coordinate systems employed for television because most of the required characteristics are comparable between proLab and competitive systems. Moreover, the criteria related to the straightness of constant tone lines are met analytically accurately due to the intrinsic property of the model.

X. DISCUSSION

A key feature of the proLab design is its projectivity. Within this color coordinate space, the central projection on any plane bypassing $\mathbf{0}$ is a chromaticity diagram, since proLab does not shift the coordinate origin. That is, colors that differ only in brightness in the original space of spectral irradiance are mapped onto a single point.

Another interesting property of proLab concerns image shot noise. In a noisy image, color estimation by arithmetic averaging is valid only in linear color spaces. However, chromaticity estimation by linear regression is invalid even in a linear space, since the amplitude of shot noise depends on the value of the color coordinates. Nevertheless, in proLab, the linear regression procedure appears to be more correct, due to the noise being more homoscedastic compared to that in standard linear spaces.

In this work, proLab was constructed for the D65 light source, so the question arises of how to adapt these color coordinates to a different kind of illumination. To achieve the best possible accuracy, we should form sample $G^2_{n_1}$ of color pairs over the given light source gamut and then optimize matrix Q on this sample. However, this procedure is inconvenient and time consuming; thus, we suggest using an approach similar to that of CIELAB: parameterization of the transformation with the light source coordinates while keeping 'the kernel' of the transformation Q the same. We find this approach to be optimal for proLab as well as for CIELAB, since for both systems the inaccuracy in uniformity is too significant to be fixed by a separate optimization. Thus, for light sources other than D65, we suggest using the same elements of the matrix Q as in (44).

For both techniques, the matrix P is finally defined in accordance with the von Kries adaptation model (9). Here, we use this simplification just for compatibility with existing solutions, taking into account that the given model is criticized for poor accuracy. Currently, several more accurate adaptation models also named after von Kries are known, which are expressed via linear transformation of the color coordinates [75]. These models could also be used in proLab, since the replacement of the adaptation model by another linear (and even projective) one does not affect the matrix Q and requires only redefinition of the matrix N.

Depending on the specific task, the metric parameters of proLab could also be modified. Particularly, it is not obvious that pairs with different color differences ΔE^*_{00} should be equally weighted while solving the optimization problem. In some possible applications, large (or small) color differences could be negligible. In these cases, the parameters of proLab must be optimized with the same method but on a different $G^2_{n_1}$ sample.

In addition, the relationship between the L^+ axis and the brightness can be weakened to increase or toughen the perceptual uniformity of the result. Alternatively, the strictness of condition (22) could be increased for LMS color coordinates. Note that the fulfillment of requirement (22) directly implies the fulfillment of similar requirements on the linRGB coordinates. All elements of the transition matrix from linRGB to CIE XYZ are non-negative, and

$$\mathbf{x} \in \mathbb{R}^n_{\geq 0}, \quad A \in \mathbb{R}^{n\times n}_{\geq 0} \Longrightarrow A\mathbf{x} \in \mathbb{R}^n_{\geq 0}, \tag{59}$$

i.e., a non-negative increment in linRGB implies a non-negative increment in CIE XYZ. Since the transformation from sRGB to linRGB is componentwise monotonic,

the aforesaid also implies that the lightness component is nondecreasing when increasing the sRGB coordinates. However, in the LMS space, the same behavior is not guaranteed, as the transformation matrix from LMS to CIE XYZ contains negative elements.

It is important to further study the parameters of noise in various spaces, including proLab. Our interest is in the experimental data for various cameras as well as the analytical models for the estimation of heteroscedasticity under various conditions. Along with shot noise, these models could consider sensor signal discreteness. Outside the context of uniform color spaces, the effects of color digitization in technical systems were already studied in [76].

We also note that the secondary locus of the joint distance chart shown in Fig. 9 raises a question regarding the localization of the significantly nonprojective parts of the gamut. On the other hand, the strict requirement of projectivity was introduced formally. In practice, the regression errors caused by the nonprojectivity of the model may turn out to be insignificant compared to the noise. Therefore, further study could also involve the construction of a low-parametric and computationally simple color model close to the projective one and with better perceptual uniformity, as well as reduced noise heteroscedasticity.

XI. CONCLUSION

ProLab is a novel color coordinate system that is demonstrated to be superior to CIELAB in perceptual uniformity while still preserving color manifold linearity. This property is not present in either CIELAB or CAM16-UCS. Reproduction angular errors can be used in proLab, as in linear color spaces. ProLab, by design, aligns angular errors of different hues to CIEDE2000 perceptual color differences, unlike the previously mentioned systems. Furthermore, we demonstrate that image noise in proLab is more homoscedastic than in other standard spaces, including linear ones. These advantages make proLab a preferred coordinate system in which to perform the structural analysis of color distributions. Because the incidence of linear manifolds is preserved, the light source direction can be estimated by the intersection of planes formed by the color distribution of glossy surfaces in proLab. Estimating manifold coordinates with no additional corrections of noise heteroscedasticity should deliver the same or better accuracy than that of standard linear spaces. Furthermore, the mutual positions of manifolds, including the angles between lines, in proLab are in correspondence with human perception.

The MATLAB/Octave implementation of proLab is available at GitHub repository github.com / konovalenko-iitp / proLab. Transformations P and P^{-1} from the CIE XYZ space to the proLab space and vice versa are implemented by functions ''XYZ2proLab.m'' and ''proLab2XYZ.m''. Optimal proLab parameters can be reproduced using the script ''search_optimal_proLab_param.m''. Results of a quantitative comparison using U_T and H_T can be reproduced via the function ''criterion_report.m''. See the ''README.md'' file for more details.

ACKNOWLEDGMENT

The authors thank Prof. Valentina Bozhkova, their colleagues at the 25th Symposium of the International Colour Vision Society, and their colleagues at Huawei Color Constancy and Multispectral Processing Workshop 2019 for the fruitful discussions of the main idea behind this work.

REFERENCES

[1] H. Grassmann, ''Zur theorie der farbenmischung,'' *Annalen der Physik und Chem.*, vol. 165, no. 5, pp. 69–84, 1853.
[2] T. Smith and J. Guild, ''The C.I.E. Colorimetric standards and their use,'' *Trans. Opt. Soc.*, vol. 33, no. 3, pp. 73–134, 1931.
[3] M. D. Fairchild, *Color Appearance Models*. Hoboken, NJ, USA: Wiley, 2013.
[4] M. R. Luo, *CIE Chromatic Adaptation; Comparison of von Kries, CIELAB, CMCCAT97 and CAT02*. Berlin, Germany: Springer, 2014, pp. 1–8.
[5] R. S. Hunter, ''Accuracy, precision, and stability of new photoelectric color-difference meter,'' *J. Opt. Soc. Amer.*, vol. 38, no. 12, p. 1094, 1948.
[6] TIC on Illumination, ''Technical note: Brussels session of the international commission on illumination,'' *J. Opt. Soc. Amer.*, vol. 50, no. 1, pp. 89–90, 1960.
[7] G. Wyszecki, ''Proposal for a new color-difference formula,'' *J. Opt. Soc. Amer.*, vol. 53, no. 11, pp. 1318–1319, 1963.
[8] K. McLAREN, ''XIII—The development of the CIE 1976 (L* a* b*) uniform colour space and colour-difference formula,'' *J. Soc. Dyers Colourists*, vol. 92, no. 9, pp. 338–341, Oct. 2008.
[9] R. G. Kuehni, ''Towards an improved uniform color space,'' *Color Res. Appl.*, vol. 24, no. 4, pp. 253–265, Aug. 1999.
[10] D. H. Alman, R. Berns, H. Komatsubara, W. Li, M. R. Luo, M. Melgosa, J. H. Nobbs, B. Rigg, A. R. Robertson, and K. Witt, ''Improvement to industrial colour-difference evaluation,'' Central Bur. Int. Commission Illumination, Vienna, Austria, Tech. Rep. Publication CIE 142-2001, 2001.
[11] M. R. Luo, G. Cui, and B. Rigg, ''The development of the CIE 2000 colour-difference formula: CIEDE2000,'' *Color Res. Appl.*, vol. 26, no. 5, pp. 340–350, 2001.
[12] H. Wang, G. Cui, M. R. Luo, and H. Xu, ''Evaluation of colour-difference formulae for different colour-difference magnitudes,'' *Color Res. Appl.*, vol. 37, no. 5, pp. 316–325, 2012.
[13] C. Li, Z. Li, Z. Wang, Y. Xu, M. R. Luo, G. Cui, M. Melgosa, M. H. Brill, and M. Pointer, ''Comprehensive color solutions: CAM16, CAT16, and CAM16-UCS,'' *Color Res. Appl.*, vol. 42, no. 6, pp. 703–718, Dec. 2017.
[14] H. C. Karaimer and M. S. Brown, ''Improving color reproduction accuracy on cameras,'' in *Proc. IEEE/CVF Conf. Comput. Vis. Pattern Recognit.*, Jun. 2018, pp. 6440–6449.
[15] G. Hong, M. R. Luo, and P. A. Rhodes, ''A study of digital camera colorimetric characterization based on polynomial modeling,'' *Color, Res. Appl.*, vol. 26, no. 1, pp. 76–84, 2001.
[16] G. D. Finlayson, M. Mackiewicz, and A. Hurlbert, ''Color correction using root-polynomial regression,'' *IEEE Trans. Image Process.*, vol. 24, no. 5, pp. 1460–1470, May 2015.
[17] S. Bianco, A. R. Bruna, F. Naccari, and R. Schettini, ''Color correction pipeline optimization for digital cameras,'' *J. Electron. Imag.*, vol. 22, no. 2, pp. 1–11, 2013.
[18] A. Kordecki, ''Practical testing of irradiance-independent camera color calibration,'' in *Proc. 11th Int. Conf. Mach. Vis. (ICMV)*, vol. 11041, Mar. 2019, pp. 340–345.
[19] J. Vazquez-Corral, D. Connah, and M. Bertalmío, ''Perceptual color characterization of cameras,'' *Sensors*, vol. 14, no. 12, pp. 23205–23229, Dec. 2014.
[20] S. A. Shafer, ''Using color to separate reflection components,'' *Color Res. Appl.*, vol. 10, no. 4, pp. 210–218, 1985.
[21] P. P. Nikolaev, ''Some algorithms for surface color recognition,'' in *Simulation of Learning and Behavior*. Moscow, Russia: Nauka, 1975, pp. 121–151.
[22] M. H. Brill, ''Image segmentation by object color: A unifying framework and connection to color constancy,'' *J. Opt. Soc. Amer. A, Opt. Image Sci.*, vol. 7, no. 10, pp. 2041–2047, 1990.

[23] D. P. Nikolaev and P. P. Nikolayev, "Linear color segmentation and its implementation," *Comput. Vis. Image Understand.*, vol. 94, nos. 1–3, pp. 115–139, Apr. 2004.
[24] G. J. Klinker, S. A. Shafer, and T. Kanade, "Image segmentation and reflection analysis through color," in *Proc. SPIE, Appl. Artif. Intell. VI*, vol. 0937, 1988, pp. 229–244.
[25] H. D. Cheng, X. H. Jiang, Y. Sun, and J. Wang, "Color image segmentation: Advances and prospects," *Pattern Recognit.*, vol. 34, no. 12, pp. 2259–2281, Dec. 2001.
[26] Y. V. Vinogradova, D. P. Nikolaev, and D. G. Slugin, "Image segmentation of color documents using color clustering," *J. Inf. Technol. Comput. Syst.*, no. 2, pp. 40–49, 2015.
[27] H.-C. Lee, "Method for computing the scene-illuminant chromaticity from specular highlights," *J. Opt. Soc. Amer. A, Opt. Image Sci.*, vol. 3, no. 10, pp. 1694–1699, 1986.
[28] J. Toro and B. Funt, "A multilinear constraint on dichromatic planes for illumination estimation," *IEEE Trans. Image Process.*, vol. 16, no. 1, pp. 92–97, Dec. 2007.
[29] J. Toro, "Dichromatic illumination estimation without pre-segmentation," *Pattern Recognit. Lett.*, vol. 29, no. 7, pp. 871–877, 2008.
[30] S.-M. Woo, S.-H. Lee, J.-S. Yoo, and J.-O. Kim, "Improving color constancy in an ambient light environment using the phong reflection model," *IEEE Trans. Image Process.*, vol. 27, no. 4, pp. 1862–1877, Apr. 2018.
[31] T. Zickler, S. P. Mallick, D. J. Kriegman, and P. N. Belhumeur, "Color subspaces as photometric invariants," *Int. J. Comput. Vis.*, vol. 79, no. 1, pp. 13–30, Aug. 2008.
[32] A. V. Nikonorov, "Spectrum shape elements model for correction of multichannel images," *Comput. Opt.*, vol. 38, no. 2, pp. 304–313, 2014.
[33] G. D. Finlayson, B. V. Funt, and K. Barnard, "Color constancy under varying illumination," in *Proc. IEEE Int. Conf. Comput. Vis.*, Jun. 1995, pp. 720–725.
[34] A. Gijsenij, T. Gevers, and J. van de Weijer, "Computational color constancy: Survey and experiments," *IEEE Trans. Image Process.*, vol. 20, no. 9, pp. 2475–2489, Sep. 2011.
[35] G. Hemrit, G. D. Finlayson, A. Gijsenij, P. Gehler, S. Bianco, B. Funt, M. Drew, and L. Shi, "Rehabilitating the colorchecker dataset for illuminant estimation," in *Proc. 26th Color Imag. Conf. Final Program*, 2018, pp. 350–353.
[36] G. Finlayson and R. Zakizadeh, "Reproduction angular error: An improved performance metric for illuminant estimation," in *Proc. Brit. Mach. Vis. Conf.*, 2014, pp. 1–11.
[37] B. Jähne, *Digital Image Processing*, 6th ed. Berlin, Germany: Springer, 2005.
[38] J. Liang, K. Xiao, M. R. Pointer, X. Wan, and C. Li, "Spectra estimation from raw camera responses based on adaptive local-weighted linear regression," *Opt. Exp.*, vol. 27, no. 4, pp. 5165–5180, 2019.
[39] G. Finlayson, H. Gong, and R. B. Fisher, "Color homography: Theory and applications," *IEEE Trans. Pattern Anal. Mach. Intell.*, vol. 41, no. 1, pp. 20–33, Jan. 2019.
[40] D. L. MacAdam, "Projective transformations of I.C.I. Color specifications," *J. Opt. Soc. Amer.*, vol. 27, no. 8, pp. 294–299, 1937.
[41] G. Wallace, H. Chen, and K. Li, "Color gamut matching for tiled display walls," in *Proc. Workshop Virtual Environ. (EGVE)*, 2003, pp. 293–302.
[42] H. Gong, G. D. Finlayson, R. B. Fisher, and F. Fang, "3D color homography model for photo-realistic color transfer re-coding," *Vis. Comput.*, vol. 35, no. 3, pp. 323–333, Mar. 2019.
[43] A. Smagina, V. Bozhkova, S. Gladilin, and D. Nikolaev, "Linear colour segmentation revisited," in *Proc. 11th Int. Conf. Mach. Vis. (ICMV)*, vol. 11041, Mar. 2019, pp. 107–119.
[44] K. Kim, T. Lim, C. Kim, S. Park, C. Park, and C. Keum, "High-precision color uniformity based on 4D transformation for micro-LED," in *Proc. SPIE, 24th Light-Emitting Devices, Mater., Appl.*, vol. 11302, 2020, Art. no. 113021U.
[45] I. Konovalenko, A. Smagina, V. Kokhan, and D. Nikolaev, "ProLab: Perceptually uniform projective colour coordinate system," in *Proc. 25th Symp. Int. Colour Vis. Society*, 2019, p. 70.
[46] P. J. Besl and D. N. McKay, "A method for registration of 3-D shapes," *IEEE Trans. Pattern Anal. Mach. Intell.*, vol. 14, no. 2, pp. 239–256, Feb. 1992.
[47] M. Stokes, M. Anderson, S. Chandrasekar, and R. Motta, "A standard default color space for the internet–sRGB, version 1.10," Int. Color Consortium, Richmond, VI, USA, Tech. Rep., 1996. [Online]. Available: http://www.color.org/sRGB.xalter
[48] J. B. Kruskal, "Multidimensional scaling by optimizing goodness of fit to a nonmetric hypothesis," *Psychometrika*, vol. 29, no. 1, pp. 1–27, Mar. 1964.
[49] P. A. Garcia, R. Huertas, M. Melgosa, and G. Cui, "Measurement of the relationship between perceived and computed color differences," *J. Opt. Soc. Amer. A, Opt. Image Sci.*, vol. 24, no. 7, pp. 1823–1829, 2007.
[50] Q. Pan and S. Westland, "Comparative evaluation of color differences between color palettes," in *Proc. 26th Color Imag. Conf. Final Program*, 2018, pp. 110–115.
[51] K. Thomsen, "A Euclidean color space in high agreement with the CIE94 color difference formula," *Color Res. Appl.*, vol. 25, no. 1, pp. 64–65, Feb. 2000.
[52] P. Urban, M. R. Rosen, R. S. Berns, and D. Schleicher, "Embedding non-Euclidean color spaces into Euclidean color spaces with minimal isometric disagreement," *J. Opt. Soc. Amer. A, Opt. Image Sci.*, vol. 24, no. 6, pp. 1516–1528, 2007.
[53] Z. Wang, B. Du, and Y. Guo, "Domain adaptation with neural embedding matching," *IEEE Trans. Neural Netw. Learn. Syst.*, vol. 31, no. 7, pp. 2387–2397, Jul. 2019.
[54] Z. Wang, B. Du, W. Tu, L. Zhang, and D. Tao, "Incorporating distribution matching into uncertainty for multiple kernel active learning," *IEEE Trans. Knowl. Data Eng.*, vol. 33, no. 1, pp. 128–142, Jan. 2019.
[55] G. Hinton, O. Vinyals, and J. Dean, "Distilling the knowledge in a neural network," 2015, *arXiv:1503.02531*. [Online]. Available: http://arxiv.org/abs/1503.02531
[56] V. V. Maximov, *Transformation of Colour Under the Changing Illumination*. Moscow, Russia: Nauka, 1984.
[57] T. Bäck, D. B. Fogel, and Z. Michalewicz, *Handbook of Evolutionary Computation*, 1st ed. Bristol, U.K.: IOP Publishing, 1997.
[58] G. Sharma, W. Wu, and E. N. Dalal, "The CIEDE2000 color-difference formula: Implementation notes, supplementary test data, and mathematical observations," *Color Res. Appl.*, vol. 30, no. 1, pp. 21–30, 2005.
[59] R. Martí, J. A. Lozano, A. Mendiburu, and L. Hernando, *Multi-Start Methods*. Cham, Switzerland: Springer, 2018, pp. 155–175.
[60] J. Nocedal and S. J. Wright, *Numerical Optimization*. Cham, Switzerland: Springer, 2006.
[61] N. Ohta and A. R. Robertson, *CIE Standard Colorimetric System*. Hoboken, NJ, USA: Wiley, 2006, ch. 3, pp. 63–114.
[62] A. Smagina, E. Ershov, and A. Grigoryev, "Multiple light source dataset for colour research," in *Proc. 12th Int. Conf. Mach. Vis. (ICMV)*, vol. 11433, Jan. 2020, pp. 635–642.
[63] D. L. MacAdam, "Visual sensitivities to color differences in daylight," *J. Opt. Soc. Amer.*, vol. 32, no. 5, pp. 247–274, 1942.
[64] A. S. Incorporated, "Adobe RGB (1998) color image encoding, version 2005-05," Corporate Headquarters, San Jose, CA, USA, Tech. Rep., 2005.
[65] M. C. Stone, "Color and brightness appearance issues in tiled displays," *IEEE Comput. Graph. Appl.*, vol. 21, no. 5, pp. 58–66, Sep./Oct. 2001.
[66] M. Bern and D. Eppstein, "Optimized color gamuts for tiled displays," in *Proc. 19th Conf. Comput. Geometry (SCG)*, 2003, pp. 274–281.
[67] A. Majumder, R. G. Brown, and H. S. El-Ghoroury, "Display gamut reshaping for color emulation and balancing," in *Proc. IEEE Comput. Soc. Conf. Comput. Vis. Pattern Recognit. Workshops*, Jun. 2010, pp. 17–24.
[68] Y. Aksoy, T. O. Aydin, M. Pollefeys, and A. Smolić, "Interactive high-quality green-screen keying via color unmixing," *ACM Trans. Graph.*, vol. 36, no. 4, p. 1, Jul. 2017.
[69] Y. Aksoy, T. O. Aydin, A. Smolić, and M. Pollefeys, "Unmixing-based soft color segmentation for image manipulation," *ACM Trans. Graph.*, vol. 36, no. 4, p. 1, Jul. 2017.
[70] N. Akimoto, H. Zhu, Y. Jin, and Y. Aoki, "Fast soft color segmentation," in *Proc. IEEE/CVF Conf. Comput. Vis. Pattern Recognit. (CVPR)*, Jun. 2020, pp. 8277–8286.
[71] S. N. Sinha, J. Kopf, M. Goesele, D. Scharstein, and R. Szeliski, "Image-based rendering for scenes with reflections," *ACM Trans. Graph.*, vol. 31, no. 4, pp. 1–10, Aug. 2012.
[72] Y. Shih, D. Krishnan, F. Durand, and W. T. Freeman, "Reflection removal using ghosting cues," in *Proc. IEEE Conf. Comput. Vis. Pattern Recognit. (CVPR)*, Jun. 2015, pp. 3193–3201.
[73] R. Carroll, R. Ramamoorthi, and M. Agrawala, "Illumination decomposition for material recoloring with consistent interreflections," *ACM Trans. Graph.*, vol. 30, no. 4, pp. 1–10, Jul. 2011.
[74] M. Safdar and M. R. Luo, "Test criteria and investigation of uniform color spaces to meet the requirements of future imagery," in *Proc. Adv. Graphic Commun. Media Technol.*, 2017, pp. 3–8.
[75] S. Bianco and R. Schettini, "Two new von Kries based chromatic adaptation transforms found by numerical optimization," *Color Res. Appl.*, vol. 35, no. 3, pp. 184–192, Jun. 2010.
[76] I. G. Palchikova, E. S. Smirnov, and E. I. Palchikov, "Quantization noise as a determinant for color thresholds in machine vision," *J. Opt. Soc. Amer. A, Opt. Image Sci.*, vol. 35, no. 4, pp. B214–B222, 2018.

IVAN A. KONOVALENKO was born in Karasuk, Novosibirsk, USSR, in 1990. He received the M.S. degree in applied mathematics and physics from Moscow Institute of Physics and Technology, Dolgoprudny, Russia, in 2014.

From 2009 to 2013, he was a Trainee Researcher with the Predictive Modeling and Optimization Laboratory, Institute for Information Transmission Problems (IITP), Russian Academy of Sciences. Since 2013, he has been a Researcher with the Vision Systems Laboratory, IITP. He has authored more than 70 articles. His research interests include computer vision, colorimetry, projective geometry, and mathematical optimization.

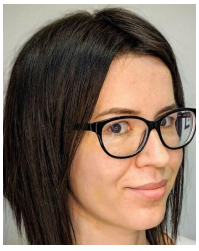

ANNA A. SMAGINA received the B.S. degree in applied mathematics and physics from Samara State Aerospace University, Russia, in 2013, and the M.S. degree in high-energy physics from Moscow Institute of Physics and Technology, Russia, in 2016. Since 2017, she has been working as a Researcher with the Vision Systems Laboratory, Institute for Information Transmission Problems, Russian Academy of Sciences (Kharkevich Institute), Moscow. She has authored more than 30 articles. Her research interests include technical color vision and 3D computer vision.

DMITRY P. NIKOLAEV (Member, IEEE) was born in Moscow, Russia, in 1978. He received the master's degree in physics and the Ph.D. degree in computer science from Moscow State University, Moscow, in 2000 and 2004, respectively.

Since 2007, he has been the Head of the Vision Systems Laboratory, Institute for Information Transmission Problems, Russian Academy of Sciences (Kharkevich Institute), Moscow, and the CTO of Smart Engines Service LLC, Moscow, since 2016. Since 2016, he has also been an Associate Professor with Moscow Institute of Physics and Technology (State University), Moscow, teaching the image processing and analysis course. He has authored over 250 scientific publications and ten patents. His research interests include the area of computer vision with primary application to color image understanding. He led a team of authors to win the Document Image Binarization Competition (DIBCO), in 2017.

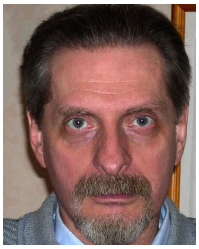

PETR P. NIKOLAEV received the degree majoring in physics from Moscow State University, in 1966, and received the Ph.D. degree, in 1975. In 1993, he was awarded as a Full Doctor of physics and mathematical sciences in the field of biophysics. Since 2015, he has been a Professor with Moscow Institute of Physics and Technology (State University), Moscow, teaching the computer vision course. He currently holds a tenured post as a Head Researcher of the Vision Systems Laboratory, Institute for Information Transmission Problems, Russian Academy of Sciences (Kharkevich Institute), Moscow, and works on the theoretical problems of color and space perception, recognition, and 3D representation. He has authored over 100 scientific publications and three books. His major scientific achievements are related to the fundamental aspects of the psychophysics of human vision, pattern recognition, and image analysis. He is a Laureate of the National Award "Russia's Outstanding Scientist."